

GEOCHEMICAL TRACES OF HISTORICAL EASTERN MEDITERRANEAN
TSUNAMIS IN THE SEDIMENTS OF ÖLÜDENİZ LAGOON, SW TURKEY

A THESIS SUBMITTED TO
THE GRADUATE SCHOOL OF NATURAL AND APPLIED SCIENCES
OF
MIDDLE EAST TECHNICAL UNIVERSITY

BY
MURAT TOYGAR YENİÇERİ

IN PARTIAL FULFILLMENT OF THE REQUIREMENTS
FOR
THE DEGREE OF MASTER OF SCIENCE
IN
GEOLOGICAL ENGINEERING

JANUARY 2020

Approval of the thesis:

**GEOCHEMICAL TRACES OF HISTORICAL EASTERN
MEDITERRANEAN TSUNAMIS IN THE SEDIMENTS OF
ÖLÜDENİZ LAGOON, SW TURKEY**

submitted by **MURAT TOYGAR YENİÇERİ** in partial fulfillment of the requirements for the degree of **Master of Science in Geological Engineering, Middle East Technical University** by,

Prof. Dr. Halil Kalıpçılar
Dean, Graduate School of **Natural and Applied Sciences** _____

Prof. Dr. Erdin Bozkurt
Head of the Department, **Geological Engineering** _____

Assist. Prof. Dr. Ulaş Avşar
Supervisor, **Geological Engineering, METU** _____

Examining Committee Members:

Prof. Dr. Nuretdin Kaymakcı
Geological Engineering, METU _____

Assist. Prof. Dr. Ulaş Avşar
Geological Engineering, METU _____

Prof. Dr. İsmail Ömer Yılmaz
Geological Engineering, METU _____

Assoc. Prof. Dr. Bora Uzel
Geological Engineering, Dokuz Eylül Uni. _____

Assist. Prof. Dr. Atilla Arda Özacar
Geological Engineering, METU _____

Date: 16.01.2020

I hereby declare that all information in this document has been obtained and presented in accordance with academic rules and ethical conduct. I also declare that, as required by these rules and conduct, I have fully cited and referenced all material and results that are not original to this work.

Name, Last name : Murat Toygar Yeniçeri

Signature :

ABSTRACT

GEOCHEMICAL TRACES OF HISTORICAL EASTERN MEDITERRANEAN TSUNAMIS IN THE SEDIMENTS OF ÖLÜDENİZ LAGOON, SW TURKEY

Yeniçeri, Murat Toygar
Master of Science, Geological Engineering
Supervisor: Assist. Prof. Dr. Ulaş Avşar

January 2020, 91 pages

Tsunami is flooding of huge wave of sea water over the land that has the potential to cause destruction and devastation on the coastal regions. They are the result of large subaqueous mass movements possibly related to earthquakes, landslides and volcanic eruptions. More than 44 tsunamis having intensities higher than 6 have been recorded historically in the Mediterranean and connected seas. In order to reveal their sedimentological traces, we investigated Ölüdeniz Lagoon, a depositional environment which has the potential to preserve the tsunami records. For this purpose, three piston cores, ca. 3.5 m-long, were collected at three different locations in the lagoon. The cores were analyzed using ITRAX-micro XRF scanner to obtain high-resolution radiographic and optical images, and element constituents of sediments as well. Six pinus branches were picked from the cores for radiocarbon dating. Eight sedimentary events are recognized along the cores based on visual inspection and interpretation of elemental profiles. These sedimentary events show [Ti, Fe, Zn]/Ca anomalies, which imply sudden sediment influx from land into the lagoon, probably from the sand spit of the lagoon. Three

of these events clearly correspond to well-known tsunamis in the eastern Mediterranean, which took place in 1609 CE, 1303 CE and 365 CE. The other four depositional events temporally correlate with less-known tsunamis in 746 CE, 148 CE and 142/143 BCE. Although sudden terrigenous sediment influx into the lagoon can be due to environmental events other than tsunamis, e.g. floods (from inland) or storm surges (from sand spit), tsunamis were accepted as “usual suspects” responsible for the sedimentary events ([Ti, Fe, Zn]/Ca anomalies) in Ölüdeniz Lagoon due to two main reasons: 1) They temporally correlate with well-known historical tsunamis, and 2) Tsunamis, rather than storms, make up the 90% of all extreme wave events in the Mediterranean for the period 1902-2017. An important observation is that all events detected in three cores do not contain any mollusk shells or gravel/pebble size materials. This means that tsunamis that hit Ölüdeniz Lagoon were not strong enough to carry coarse material even for 300-400 m from the sand spit to the middle parts of the lagoon (coring locations). It seems that tsunamis in the eastern Mediterranean Sea are not as catastrophic as the ones in the Indian and Pacific oceans.

Keywords: Paleotsunami, Eastern Mediterranean, Ölüdeniz Lagoon, ITRAX micro-XRF Core Scanning, Radiocarbon Dating.

ÖZ

DOĞU AKDENİZ TARİHSEL TSUNAMİLERİNİN ÖLÜDENİZ LAGÜNÜ (GB TÜRKİYE) SEDİMANLARI İÇİNDEKİ JEOKİMYASAL İZLERİ

Yeniçeri, Murat Toygar
Yüksek Lisans, Jeoloji Mühendisliği
Tez Yöneticisi: Dr. Öğr. Üyesi Ulaş Avşar

Ocak 2020, 91 sayfa

Tsunami, dev deniz dalgalarının kıyı bölgelere taşmasıyla meydana gelen ve ciddi yıkımlara sebep olabilen bir doğa olayıdır. Bu devasa dalgaların sebebi, deprem, heyelan yada volkanik patlama nedeni ile oluşan ani sualtı kütle hareketleridir. Akdeniz ve ona bağlı denizlerde meydana gelmiş ve tarihsel kayıtlara geçmiş şiddeti 6'dan büyük 44 adet tsunami vardır. Bu çalışma, Doğu Akdeniz'de meydana gelmiş tsunamilerin sedimanter izlerini araştırmak için yapılmıştır. Tsunamileri sedimantolojik olarak kaydetme potansiyeli yüksek bir çökelim ortamı olan Ölüdeniz Lagünü'nden, uzunlukları yaklaşık 3.5 metre olan üç adet piston karot alınmıştır. Yüksek çözünürlüklü radyografik ve optik görüntülerin, ve sedimanların jeokimyasal içeriklerinin elde edilmesi için, karotlar ITRAX mikro-XRF cihazı ile taranmıştır. Altı adet bitki kalıntısı (muhtemelen çam ağacı parçası) radyokarbon tarihlendirmesi için kullanılmıştır. Yapılan analizler ve sedimantolojik incelemeler sonucunda, Ölüdeniz istifinde sekiz adet sedimanter olay tespit edilmiştir. Tespit edilen sedimanter olaylar, lagüne ani karasal sediman girişini gösteren (muhtemelen kum bariyerden) [Ti, Fe, Zn]/Ca anomalileri olarak karşımıza çıkmaktadır. Radyokarbon tarihlendirmesine dayanan sediman

kronolojisine göre, bu olaylardan üçü, M.S. 1609, M.S. 1303 ve M.S. 365 yıllarında meydana gelmiş ve iyi bilinen tarihsel tsunamiler ile zamansal olarak uyumaktadır. Diğer dört olayın ise, tarihsel kayıtlarda bulunan M.S. 746, M.S. 148 ve M.Ö. 142/143 tsunamileri ile ilişkili olduğu düşünülmektedir. Bir lagüne ani karasal sediman girişlerinin, tsunami haricinde sel ve fırtına kabarması gibi olaylar ile de olabileceği düşünülse de, tsunamileri Ölüdeniz'deki sedimanter olaylar için "olağan şüpheli" olarak kabul etmemizi sağlayan iki ana neden vardır: 1) Olayların tarihleri tarihsel tsunamiler ile deneştirilebilmektedir, ve 2) 1902-2017 döneminde Akdeniz'de meydana gelen şiddetli dalga olaylarının %90'ı fırtınalardan ziyade tsunamilerdir. Bu çalışmada yapılan bir diğer önemli gözlem ise; üç karotta tespit edilen sedimanter olayların hiçbirinde molusk kabuğu yada çakıl gibi iri taneli malzemenin bulunmamasıdır. Ölüdeniz Lagünü'nü vuran tsunamiler, iri taneli malzemeyi kum bariyerden lagünün 300-400 metre iç kısımlarına taşıyacak kadar güçlü değildir. Bu da; Doğu Akdeniz'deki tsunamilerin, Hint ve Pasifik okyanuslarında meydana gelen tsunamiler kadar yıkıcı olmadığını bir göstergesidir.

Anahtar Kelimeler: Eski Tsunami kayıtları, Doğu Akdeniz, Ölüdeniz Deniz Kulağı, ITRAX mikro-XRF taraması, Radyokarbon tarihlendirmesi

To my wife, parents and brother

ACKNOWLEDGMENTS

This study, supported by the European Commission “Marie Skłodowska-Curie Actions – Individual Fellowships” program, was carried out within the scope of “Towards a paleotsunami chronology in the southern Aegean and Levantine seas, Eastern Mediterranean (EASTMED-PALEOTSUNAMI)” project (#706671) hosted by the Geological Engineering Department of METU.

First of all, I would like to thank my supervisor Assist. Prof. Dr. Ulaş Avşar for his valuable supports during the study. I am deeply grateful for his guidance and patience.

I would also like to thank Zeynep Bektaş, for u-channel extraction and data analyses processes. While taking cores, I appreciate with their invaluable help of Assoc. Prof. Dr. Özgür Avşar, Bülent Tokay, Levent Tosun and Akın Çil.

Finally, I would like to thank my parents, Semra and Serdal Yeniçeri, my brother, Muhammed Alperen Yeniçeri, my wife Ebru Yeniçeri and my uncle Barış Yeniçeri for their inexhaustive supports during my educational life. I am also grateful for their patience and unconditional support.

TABLE OF CONTENTS

ABSTRACT.....	v
ÖZ	vii
ACKNOWLEDGMENTS	x
TABLE OF CONTENTS.....	xi
LIST OF TABLES	xiii
LIST OF FIGURES	xiv
CHAPTERS	
1 INTRODUCTION	1
1.1 Tsunami	1
1.2 Motivation: State-of-the-art Paleotsunami Research	10
1.3 Study Area.....	16
1.4 Methods.....	19
1.4.1 Bathymetric Map	19
1.4.2 Piston Coring	20
1.4.3 ITRAX micro-XRF Core Scanning	23
1.4.4 Radiocarbon Dating	28
1.4.5 Temporal Correlation with Historical Records.....	30
2 LITERATURE REVIEW	33
2.1 The Eastern Mediterranean Tsunamis.....	33
2.2 Previous Studies	35
3 RESULTS	51
3.1 Visual Inspection of the Cores	51
3.2 Micro-XRF Data	57

3.3	Radiocarbon Data	59
4	DISCUSSION.....	63
5	CONCLUSION	75
	REFERENCES	77

LIST OF TABLES

TABLES

Table 1.1 Regional and local tsunamis causing deaths since 1975 (IOC, 2016).....	6
Table 1.2 Regional and local tsunamis all time, causing 2,000 or more deaths. (IOC, 2016).....	7
Table 1.3 Brief information on the cores taken from Ölüdeniz Lagoon.....	23
Table 2.1 Historically known strong tsunamis (having intensities higher than 6) in the Mediterranean and connected seas (Papadopoulos et al., 2014). The ones having the potential to be felt around Ölüdeniz Lagoon are highlighted.....	34
Table 3.1 Information on the radiocarbon samples and dating results.	60

LIST OF FIGURES

FIGURES

- Figure 1.1. Global historical tsunami catalogue for the period from 2000 BCE to the present. Total of 2100 tsunamis has been recorded during the last 4000 years. (Gusiakov, 2009)2
- Figure 1.2. a) Main triggering mechanisms for tsunamis, according to Gusiakov (2009). Atmospheric disturbances and cosmic impacts are included in other reasons. b) Tsunami source types, according to Papadopoulos (2016). ER: earthquake; EA: earthquake associated; EL: earthquake landslide; ES: earthquake marine slide; VO: volcanic activity; VS: volcanic marine slide; UN: unknown; GL: gravity landslide; GS: gravity marine slide; ER(SQ): Seaquake.....3
- Figure 1.3. Illustration of changes in velocity, length and height of tsunami waves with respect to water depth (Röbke and Vött, 2017).....4
- Figure 1.4. Coastal depositional environments that can be targeted to find sedimentary records of past tsunamis. Modified from Jones (2001)..... 11
- Figure 1.5 a) The number of papers per year in the “Web of Science” database; Black Line: all papers using the keywords of “Tsunami+Deposit+Sediment” (total of 676); Green Line: the papers of which main focus is sedimentological investigations (total of 285); Red Line: the papers presenting paleotsunami chronologies (total of 85). The “real” sedimentological studies (pie chart) comprise 172 papers focusing on the deposits of only “single events”, 85 paleotsunami papers, and 28 review papers. b) and c) Among the paleotsunami studies, comparison of papers on coring vs. trenching, and different depositional environments in terms of the number of detected tsunamis and their mean recurrences per study. The studies are sorted along the x-axis. (From Avcı, 2019b) 13
- Figure 1.6. Different methods used in sedimentological investigations on tsunami deposits versus the number of papers used them. Note that high-resolution micro-

XRF core scanning and u-channel X-ray radiography, the main techniques applied in this study, has not been used commonly.....	15
Figure 1.7. a) Geological units and active fault systems around the study area, SW Turkey (Kaymakcı et al., 2018), b) Fault types near the vicinity of Ölüdeniz lagoon within about 40 km (MTA, 1997 ,1/250000 Scale Geological Maps of Turkey, No:2 Fethiye; Emre et al., 2018; Tosun, 2018).....	18
Figure 1.8. a) Active fault map around Ölüdeniz Lagoon Emre et al. (2011). Instrumentally recorded earthquakes ($M_w \geq 4$) around the lagoon during 1900–2020 are also shown (KOERI-NEMC EQ Catalog - http://www.koeri.boun.edu.tr). b) Close-up view to the catchment of Ölüdeniz Lagoon and the lithology on relief-shaded map (Şenel, 1997)	19
Figure 1.9. a) Sediment coring platform JEOLODTÜ. b) The route followed for bathymetric measurements. c) Bathymetric map of Ölüdeniz Lagoon and coring locations. While stars represent coring locations of Avşar (2019a), white dots represent coring locations of this study.....	20
Figure 1.10. Schematized steps of piston coring operation (Avşar, 2013)	22
Figure 1.11. Principles of ITRAX micro-XRF core scanning, (a) Components of ITRAX micro-XRF system (Croudace et al., 2006). A: optical line-scan camera, B: triangular laser system, C: motorized XRF Si-drift chamber detector, D: 3 kW X-ray tube, E: flat-beam X-ray waveguide, and F: The X-ray line camera. (b) A typical XRF spectrum produced by ITRAX (from Liang et al., 2012). (c) Example of RGB image, radiograph and Ti profile produced by ITRAX (from Boraboy Lake, Avşar et al., 2015).	24
Figure 1.12. a) and b) Comparison of half-core and u-channel radiographies. c) Schematic illustration of steps to extract u-channels from split-cores. d) View of a split-core after sediments on both sides of the u-channel were removed. “c” and “d” are from Avşar (2019b).....	26
Figure 2.1. Possible tectonic tsunami sources (Hellenic Arc, Cyprus Arc, Pliny & Strabo trenches and Dead Sea Fault; simplified from Barka and Reilinger, 1997), historical tsunamis (from Salamon et al., 2007 and Papadopoulos et al., 2014), and	

study sites of geological records of past tsunamis in the Eastern Mediterranean. Ölüdeniz Lagoon is well located to evaluate past tsunamis in the eastern Mediterranean..... 36

Figure 3.1. Optical and radiographic images of the cores OLD-1, OLD-2 and OLD-4. Grayscale profiles of along radiographic images and Red/Green ratio profiles along RGB images are also presented. Blue lines illustrate levels that can be correlated even based on core images. Widths of images are three times exaggerated in order to ease visual inspection. 52

Figure 3.2. Close-up view for OLD-1 optical image..... 53

Figure 3.3. Close-up view for OLD-2 optical image..... 54

Figure 3.4. Close-up view for OLD-4 optical image..... 55

Figure 3.5. XRF data for each element obtained from OLD -1, OLD -2 and OLD-4. R/G and X-ray grayscale curves are also provided. 58

Figure 3.6. Radiocarbon calibration results from Oxcal software with Intcal13 calibration curve. 61

Figure 4.1. a) Correlation of three cores by means of Ti/Ca profiles. Locations of radiocarbon dates (R1 to R6) are also shown. Note that the longest sequence is covered by OLD-2. b) Different proxies of three cores overlapped after modifying depth scales of OLD-1 and OLD-4 with respect to OLD-2. The success of stratigraphical correlation is obvious. Presence of eight sedimentary events (Grey bars 1 to 8) can be proposed. 64

Figure 4.2. Correlation of K/Ca and Ti/Ca profiles of Avşar (2019a) with the profiles of this study. 65

Figure 4.3. Age-depth curve constructed based on radiocarbon dates and correlation with the record of Avşar (2019a). At depths corresponding to the anomalies along Ti/Ca profile, the age-depth curve is vertical, meaning that these anomalies are assumed to be sudden depositional events. 66

Figure 4.4. A mechanism explaining the possible relation between tsunamis and Ti/Ca anomalies in Ölüdeniz sedimentary sequence..... 68

Figure 4.5. a) Historical tsunamis in the eastern Mediterranean and geological paleotsunami records (Yellow diamonds) (See Figure 2.1 for the legend) b) Comparison of sedimentary events (Ti/Ca anomalies) with historical tsunamis and paleotsunami records. 71

CHAPTER 1

INTRODUCTION

1.1 Tsunami

Throughout history, humanity has met many natural and fatal disasters which intertwined with mythology and religion, e.g. Sodom & Gomorrah and Noah Flood. Earth is in a constant move tectonically and meteorologically, which are responsible for such disasters; floods, earthquakes, volcanic eruptions, typhoons and tsunamis. Amongst these disasters, tsunami finds itself at fifth rank with an estimated 700,000 fatalities for all historical times (Gusiakov, 2009). Especially, the 26 December 2004 Sumatra Tsunami has reminded us once again how seriously tsunamis can threaten our lives and infrastructures. The Sumatra (Indonesia) offshore earthquake (Mw 9.1) triggered the most devastating tsunami in the recorded history and killed 230,000 people. Seven years later, on 11 March 2011, the Tohoku (Japan) offshore megathrust earthquake (Mw 9.0) triggered another tsunami resulted in 16,000 deaths and 2,600 people missing. These two tsunamis attracted the attention of the scientific community, and the number of studies aiming to find the history of tsunamis has significantly increased recently.

Tsunami terminologically means inundating huge waves over land. During history, it has got different names from different cultures. However, the term, which is globally used and known today, is “Tsunami”. It is originated from two Japanese words *tu* (port) *nami* (long wave) (Imamura, 1937). Of all over the tsunamis occurred in the world history, 56% were in the Pacific Ocean (Gusiakov, 2009). Pacific is surrounded by tectonically active structures that are responsible for almost 90% of all earthquakes and 75% of all volcanic activity on Earth. Total of

2100 tsunamis is estimated to have happened for the last 4000 years, where almost 550 of them took place in the Mediterranean Sea (Figure 1.1).

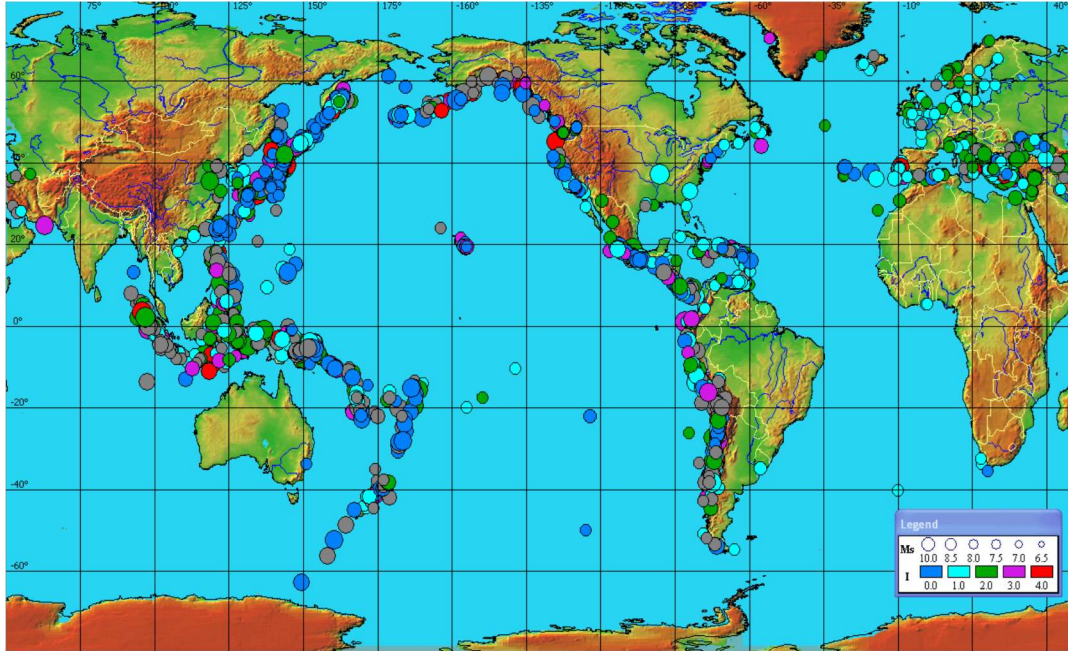


Figure 1.1. Global historical tsunami catalogue for the period from 2000 BCE to the present. Total of 2100 tsunamis has been recorded during the last 4000 years. (Gusiakov, 2009)

Tsunami occurs as a result of sudden displacement of water column (Sugawara et al., 2008; R bke and V tt, 2017), and is composed of series of sea waves with long-period and long wavelength (Papadopoulos, 2014). The main reason for this kind of wave series is tectonics; i.e. faulting associated sudden displacement of the seafloor (Sugawara et al., 2008; Gusiakov, 2009; Papadopoulos, 2016). According to Gusiakov (2009), 75% of tsunamis is of tectonic origin (Figure 1.2a). On the other hand, Papadopoulos (2016) claims that the percentage of earthquake-related tsunamis is about 82% (Figure 1.2b). In either way, tectonic activity is explicitly seen being the most important mechanism triggering tsunamis. Type of faulting also plays an important role in producing a tsunami. While dip-slip motion with dominant normal/reverse component can produce devastating tsunamis, the tsunami activity is significantly low in areas dominated by active strike-slip

faulting (even they have high seismicity), such as in the central Ionian Sea and the North Aegean Sea trough (Papadopoulos, 2016). In addition to active tectonics, there are also some mechanisms triggering tsunamis, which are landslides, submarine volcanic activities, atmospheric disturbances (meteotsunamis) and cosmic impacts (Röbke and Vött, 2017).

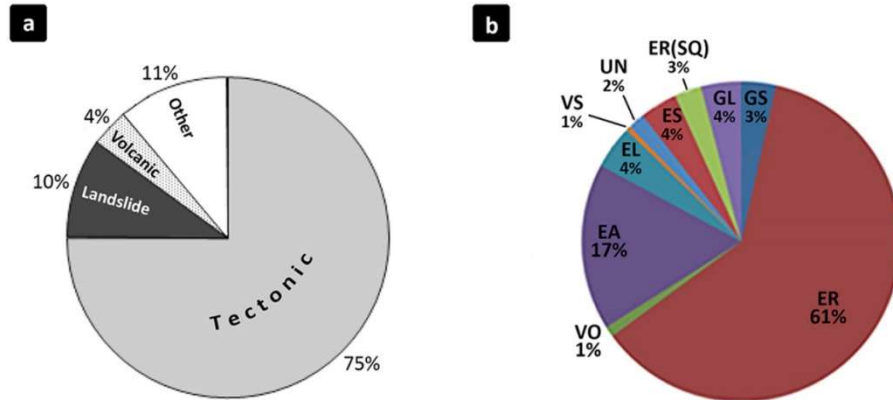


Figure 1.2. a) Main triggering mechanisms for tsunamis, according to Gusiakov (2009). Atmospheric disturbances and cosmic impacts are included in other reasons. b) Tsunami source types, according to Papadopoulos (2016). ER: earthquake; EA: earthquake associated; EL: earthquake landslide; ES: earthquake marine slide; VO: volcanic activity; VS: volcanic marine slide; UN: unknown; GL: gravity landslide; GS: gravity marine slide; ER(SQ): Seaquake

A tsunami can be considered as a shallow-water wave (Helene and Yamashita, 2006; Röbke and Vött, 2017). In the open ocean, tsunami wavelength may reach up to 500 km (Helene and Yamashita, 2006), but wave heights are generally limited to a few meters; hence it may not be thoroughly felt in open ocean (Figure 1.3) (Sugawara et al., 2008; Röbke and Vött, 2017). However, as the wave gets close to more restricted coastal waters, wave-height may increase up to several tens of meters (Dawson, 2007; Sugawara et al., 2008; Papadopoulos, 2016), and intensity of tsunami starts to be damaging. In contrast, the velocity of tsunami waves is considerably higher in the open ocean. As the waves reach the shallower environment, their velocity decreases (Figure 1.3). The velocity of waves is

proportional to gravity and water depth, and independent with wave-length/wave-height (Röbke and Vött, 2017). As water depth decreases, wave velocity decreases as well, and wave height increases to keep the total energy constant (Helene and Yamashita, 2006; Sugawara et al., 2008; Papadopoulos, 2016). Hence, the increase in wave height as tsunami approaches to shoreline results in seawater inundation on land, which may cause significant damage.

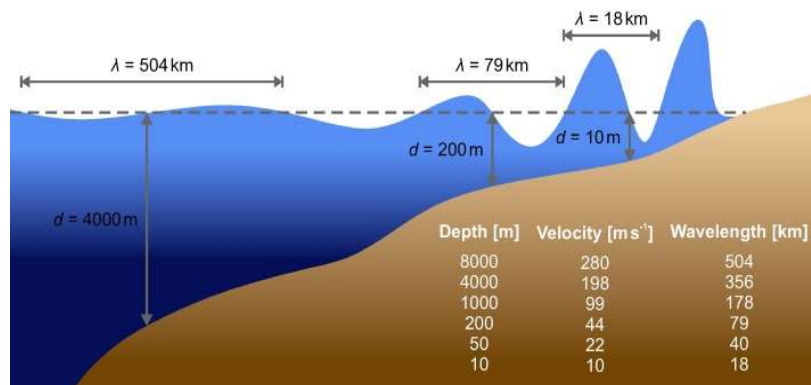


Figure 1.3. Illustration of changes in velocity, length and height of tsunami waves with respect to water depth (Röbke and Vött, 2017)

Run-up and inundation level has remarkable importance in terms of public safety. While making tsunami hazard assessment, these terms are considered because these measurements help to understand where tsunami's effects can reach on land and possibly harm effects on facilities. In recent tsunamis, in Tohoku, tsunami waves propagated more than 5 km toward inland; with maximum inundation height and mean inundation height were 19.5 and 10 meters, respectively. Their maximum run-up heights were measured as more than 20 m along the 290 km coastal area and more than 10 m along the 425 km coastal area, in the direct distance. Tsunami wave heights reached up to almost 40 m (Mori et al., 2011). In Sumatra, maximum run-up was measured in Lhoknga as 31 m, and maximum inundation was more than 3 km inland (Borrero et al., 2006). In addition, Tsuji et al. (2005) state maximum run-up was 34.8 m, tsunami wave-height was 15 to 30 m, and the inundation level was 5 to 6 km toward inland for Sumatra tsunami. Sugawara et al. (2016) also remarked that maximum tsunami wave-height exceeded 30 m during

the Sumatra tsunami. Amongst all tsunamis recorded in the world, one of the greatest run-up height was measured as 524 m in Lituya Bay, Alaska, in 1958, which was triggered by a falling rock mass of 30.5×10^6 m³ from 600-900 m altitudes (Fritz et al., 2009).

Damages of tsunami inundations can be examined in terms of three aspects; survival, economic, and environmental. Economic losses are generally due to physical damages on infrastructures in coastal areas, and on boats/ships within ports, harbors and marinas. At the economic point of view, considering recent and the most destructive tsunamis, Sumatra has approximately 20 billion \$ and Tohoku has nearly 210 billion \$ damage loss. In different sources, these numbers range from \$15 billion to \$80 billion for the Indian Ocean tsunami (Bryant, 2008) and up to \$335 billion for Tohoku tsunami (Daniell and Vervaeck, 2012). In both events, it is explicitly seen that tsunami disaster may cause significant economic losses for the countries. Tohoku tsunami also pointed out that, among the other human-made structures, nuclear power plants are probably the most dangerous facilities to be constructed at coastal sites prone to tsunami hazard. The 2011 Tohoku tsunami triggered the Fukushima nuclear disaster, which caused the largest discharge of radiation into an ocean in the history of the world. In the region, over 120,000 people evacuated from their homes and lived with the fear of radiation for years (Eddy and Sase, 2015). Notably, the Tohoku tsunami was recorded as the most expensive natural disaster in the world (Allmann, 2012; R bke and V tt, 2017).

In terms of survival view, according to research conducted by Intergovernmental Oceanographic Commission (IOC), there has been almost 260,000 fatalities due to tsunamis since 1975 (Table 1.1). If we consider tsunamis causing 2000 or more fatalities for all over the world during the whole history, this number increases up to approximately 519,000 (Table 1.2) (IOC, 2016). On the other hand, Gusiakov (2009) claims 700,000 fatalities due to tsunamis so far. However, this study was done before the Tohoku event; thus, when we add Tohoku fatality number to the cumulative amount, it approaches about 720,000. Although the fatality numbers are

different between different researchers, it is evident that this disaster has a significant impact on human life.

Table 1.1 Regional and local tsunamis causing deaths since 1975 (IOC, 2016)

Year	Month	Day	Source Location	Estimated Deaths or Missing
1975	10	31	Philippine Trench	1
1975	11	29	Hawaii, USA	2
1976	8	16	Moro Bay, Philippines	4376
1977	8	19	Sumbawa, Indonesia	189
1979	7	18	Lembata Island, Indonesia **	1239
1979	9	12	Irian Jaya, Indonesia	100
1979	10	16	French Riviera **	9
1979	12	12	Narino, Colombia *	600
1981	9	1	Samoa Islands	2
1983	5	26	Noshiro, Japan	100
1988	8	10	Solomon Islands	1
1991	4	22	Limon, Costa Rica	2
1992	9	2	Off coast Nicaragua	170
1992	12	12	Flores Sea, Indonesia	1169
1993	7	12	Sea of Japan	208
1994	6	2	Java, Indonesia	250
1994	10	8	Halmahera, Indonesia	1
1994	11	4	Skagway Alaska, USA **	1
1994	11	14	Philippine Islands *	81
1995	5	14	Timor, Indonesia	11
1995	10	9	Manzanillo, Mexico	1
1996	1	1	Sulawesi, Indonesia	9
1996	2	17	Irian Jaya, Indonesia	110
1996	2	21	Northern Peru	12
1998	7	17	Papua New Guinea	2205
1999	8	17	Izmit Bay, Turkey	155
1999	11	26	Vanuatu Islands	5
2001	6	23	Southern Peru	26
2004	12	26	Banda Aceh, Indonesia *^	227.898
2005	3	28	Sumatra, Indonesia	10
2006	3	14	Seram Island, Indonesia	4
2006	7	17	Java, Indonesia	802
2007	4	1	Solomon Islands *	52
2007	4	21	Southern Chile	10
2009	9	29	Samoa Islands	192
2010	1	12	Haiti	7
2010	2	27	Southern Chile	156
2010	10	25	Mentawai, Indonesia	431
2011	3	11	Tohoku, Japan *^	18.717
TOTAL				259,314
* May include earthquake deaths				
** Tsunami generated by landslide				
^ Includes dead/missing near and outside source region				

Table 1.2 Regional and local tsunamis all time, causing 2,000 or more deaths.
(IOC, 2016)

Year	Month	Day	Source Location	Estimated Deaths or Missing
365	7	21	Crete, Greece	5700
887	8	2	Niigata, Japan	2000
1341	10	31	Aomori Prefecture, Japan	2600
1498	9	20	Enshunada Sea, Japan	31000
1570	2	8	Central Chile	2000
1586	1	18	Ise Bay, Japan	8000
1605	2	3	Nankaido, Japan	5000
1611	12	2	Sanriku, Japan	5000
1674	2	17	Banda Sea, Indonesia	2244
1687	10	20	Southern Peru *	5000
1692	6	7	Port Royal, Jamaica	2000
1703	12	30	Boso Peninsula, Japan	5233
1707	10	28	Enshunada Sea, Japan	2000
1707	10	28	Nankaido, Japan *	5000
1746	10	29	Central Peru	4800
1751	5	20	Northwest Honshu, Japan	2100
1755	11	1	Lisbon, Portugal *	50000
1771	4	24	Ryukyu Islands, Japan	13486
1792	5	21	Kyushu Island, Japan	5443
1854	12	24	Nankaido, Japan *	3000
1868	8	13	Northern Chile *	25000
1883	8	27	Krakatau, Indonesia **	36000
1896	6	15	Sanriku, Japan *	27122
1899	9	29	Banda Sea, Indonesia	2460
1923	9	1	Sagami Bay, Japan	2144
1933	3	2	Sanriku, Japan	3022
1945	11	27	Makran Coast, Pakistan	4000
1952	11	4	Kamchatka, Russia	4000
1976	8	16	Moro Gulf, Philippines	4376
1998	7	17	Papua New Guinea	2205
2004	12	26	Banda Aceh, Indonesia *^	227898
2011	3	11	Tohoku, Japan *^	18717
TOTAL				518.550
* May include earthquake deaths				
** Tsunami generated by landslide				
^ Includes dead/missing near and outside source region				

At environmental point of view, tsunami poses a massive threat to coastal environments and ecosystems. Cultivated agricultural activities nearby coasts are subjected to severe impact from the tsunami disaster. Productive soils are swept away, as well as currently existing products during overwashing of huge waves

onto land. Inundating sea waves leave dirt behind and contaminate soil by increasing salt amount on the land. Such effects cause significant decrease in productivity. McLeod et al. (2010) argue that the crop yield will decrease for several years due to salinity of water despite hundreds of millimeters of rain in the region that help to leach the salinity.

In addition to its effects on the surface, seawater inundation due to tsunamis has also effects under the ground. As the seawater penetrates towards the deeper part of the earth, it meets with groundwater and increases the salt concentration of groundwater. Since groundwater percolates under the ground, spread this contamination many kilometers away.

Groundwater has a critical role in terms of water supply in human life (Villholth et al., 2011). It severely affects people who consume for farming. After the Sumatra Disaster, recovery duration was calculated as up to 15 years based on seven different groundwater models (Villholth et al., 2011). For human life, this time-span is long enough, especially, when we consider that 41% of Indonesia population works in agriculture, which corresponds to 14.1% of GDP of Indonesia (DEIK, 2014). Farmers and their families must have suffered from this situation. Agricultural activities indirect effect can be observed in industrial areas, such as textile and food. Since raw materials for textile and foods are grown up on farms, these sectors and similar industries which use farming products are likely to be severely affected. Besides, in the Tohoku tsunami, the Fukushima nuclear power plant was ruined due to tsunami waves. Tokyo Electric Power (Tepco) declared that the collective exposure dose of 12,000 workers at the facility had been increased before the disaster in a year. Also, within 20 km of the power plant, many people have been subjected to radiation before evacuation. While 1-2-year-old children had between 580 millisieverts and 1580 millisieverts radiation dose, this number was between 310 and 860 mSv for adults (McCurry, 2013). The estimated amount of emitted radioactivity was about 15% of the Chernobyl disaster (Baba, 2013). Besides, Tohoku tsunami caused breaking off icebergs from Sulzberger Ice Shelf icebergs in Antarctica and is responsible for killing 110,000

nesting seabirds at the Midway Atoll National Wildlife Refuge while crossing the Pacific Ocean in 5 foot-size waves (Oskin, 2017).

On coastal ecosystems; almost all of the fish or other animals consumed by people live near the coasts. Waves are not only above the surface but flowing current also beneath the water shows its impact in close enough the shore. When they come towards land, they hit nearshore and may destroy every living creature and their nesting areas in the water, on coasts and near shore. Sea products, which are used for exportation and domestic consumption, are vanished for a while, and the fisheries will also be affected. In Indonesia and Sri Lanka, many boats, fishing gear, ponds and support installations, used for fishing and aquaculture, were also destroyed due to tsunami (FAO, 2007). Fisheries in Indonesia comprise 2.5% of the GDP (DEIK, 2014). According to FAO (2018), while the number of fisheries in Indonesia is 3.1 million in 2000 and 203 thousand in Japan in 2010, these numbers decreased to 2.59 million in Indonesia in 2005 and 174 thousand in Japan in 2012 after the tsunamis. This damage can be evaluated in terms of not only fisheries but also aquaculture, which consists of aquatic organisms including fish, mollusks, crustaceans, aquatic plants, finfishes, amphibians, freshwater turtles and other aquatic animals (such as sea cucumbers, sea urchins, sea squirts and edible jellyfish), produced for consumption intend (FAO, 2014). In Sumatra Earthquake, not only Indonesia but also Sri Lanka, Maldives and India are affected. In Sri Lanka, there were 15307 motorized vessels before the tsunami. However, this number decreases to 6700 vessels aftermath of the disaster (FAO, 2010), which corresponds to about 44% losses. This disaster costs about 1 billion \$ for Sri Lanka, corresponding 4.5% of GDP, including infrastructure, private assets and equipment for fishing etc. (World Bank, 2005). In the Maldives, economic losses, as a result of the tsunami, are estimated between \$310 – \$510 million which is about 50 to 80% GDP of Maldives (World Bank, 2005). In 2011 Tohoku Tsunami, 25,000 fishing vessels, 319 fishing harbors and 1725 common use facilities were destroyed. These losses correspond to ¥170 billion, ¥823 billion and ¥124.9 billion,

respectively. Besides, aquaculture facilities and products' losses were ¥738 million and ¥575 million, respectively (World Bank, 2012).

1.2 Motivation: State-of-the-art Paleotsunami Research

The examples, as mentioned earlier, make tsunami hazard assessment studies crucial to mitigate their devastating consequences, as in the case of successfully applied in probabilistic seismic hazard assessment (PSHA) analyses. However, compared to the number of seismological datasets used in PSHA analyses, the number of known tsunamis is relatively low, which prevents developing standard and low-uncertainty statistical approaches such as PSHA analyses (Papadopoulos et al., 2014; Avşar, 2019a). PSHAs make predictions on fault behaviour mostly based on instrumentally recorded seismicity. In addition, they use paleoseismic information obtained by investigating faulting-related geological archives, i.e. on-fault trenching.

On the other hand, the number of well-known tsunamis is relatively low (Papadopoulos et al., 2014), which prevents developing standard and low-uncertainty statistical approaches like in PSHAs using seismological data. Furthermore, the on-fault trenching techniques used to evaluate the paleoseismic and tsunamigenic potential of offshore faults cannot be applied. However, to assess the frequency of tsunamis for a region, historical records are invaluable. The quality and completeness of historical tsunami records from around the world may differ substantially (Avşar, 2019a). Historical records generally do not extend back in time long enough to determine the recurrence of tsunamis accurately. Even the historical records for a region cover long time interval they still may be incomplete because of various reasons such as the tsunamis in uninhabited areas might not be reported, and the records might be lost due to political instabilities or tsunamis themselves may cause the loss of the records (Hadler et al., 2012). Thus, sedimentological and geochronological investigations on the geological archives of

coastal and nearshore depositional environments are crucial to complete the tsunami records and to determine the frequency of tsunami events (Avşar, 2019a).

Coastal depositional environments, where the tsunamis are potentially recorded include mainly lagoons, alluvial plains, back-barrier wetlands, coastal fluvial plains, tidal wetlands and enclosed water bodies, near-shore shelf and offshore deep marine environments (Figure 1.4). In terrestrial environments, deposits are vulnerable to any surface weathering conditions (flood, wind erosion, etc.), which may result in loss of tsunami records and cause incomplete sedimentary record. Amongst all, aquatic environments, especially coastal lakes and lagoons (Sugawara et al., 2008, Avşar, 2019a), are the most suitable systems, which has a higher potential for preserving depositional records of tsunami events. Tsuji et al. (2002) suggest that smaller ponds should be preferred for the sampling of tsunami deposits because the larger ones may have been subjected to human activities because of interest of people on such big water bodies (fishing etc.). Kempf et al. (2017) also suggest that hydro-dynamically active sedimentary environments tend to be altered. For long paleotsunami records, researchers need to prefer small coastal lakes (lagoons) in order not to miss any event.

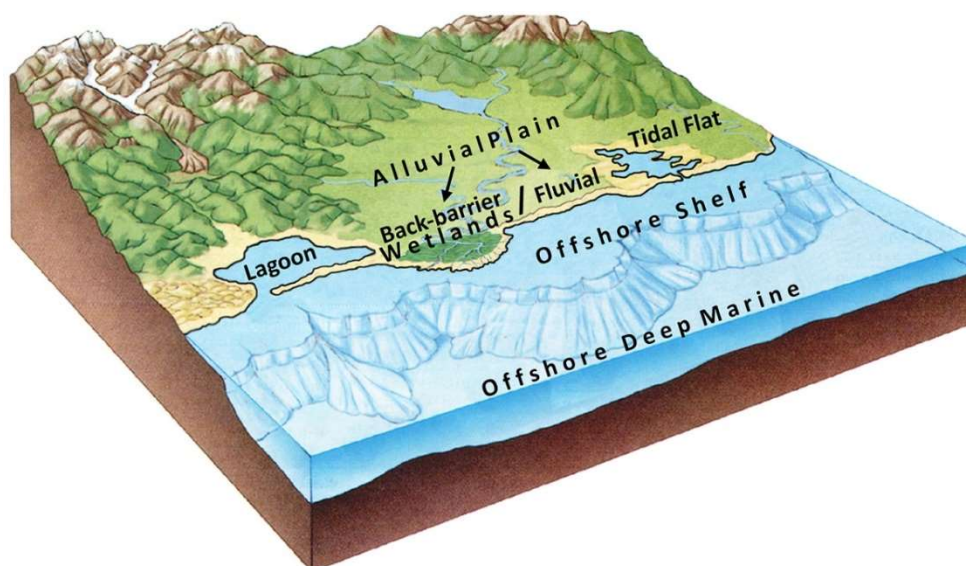


Figure 1.4. Coastal depositional environments that can be targeted to find sedimentary records of past tsunamis. Modified from Jones (2001).

When high-energy tsunami waves reach the coast, they can remobilize significant amounts of material from the areas near the shoreline and transport them towards inland during the “inflow”. The remobilized material can vary in grain-size from clay to boulders of several meters in diameter and are deposited on terrestrial lowlands as inflow deposits. They tend to get finer and thinner towards inland (e.g. Chagué-Goff et al., 2012). “Backflow” deposits, on the other hand, are relatively rare since the strength of the backflow, and hence its erosional and depositional potential is the function of the coastal topography (Bahlburg and Spiske, 2012). If backflow is strong enough, it can also erode and transport material from the lowlands towards the sea. Tsunami inflow and backflow deposits are most commonly found as sandy layer intercalations within coastal lowland stratigraphic sequences, which are investigated mostly through on-land coring and trenching techniques. Somehow, the number of sedimentological investigations employing coring in coastal aquatic environments (e.g., lagoons, nearshore shelf and deep marine) is very limited (Avşar, 2019a).

Regarding the state of paleotsunami research in the literature, Avşar (2019b) presents valuable statistical information and reveal general trends in the tsunami research in the literature (Figure 1.5). Accordingly, a preliminary search on the “Web of Science” database done by using the “Tsunami+Deposit+Sediment” keywords results in a total of 676 papers. Immediate increase in the number of papers after the 2004 Sumatra and the 2011 Tohoku tsunamis is pronounced (Figure 1.5a). Among these studies, 285 papers are focused only on the sedimentological aspects of tsunami deposits. The papers concentrate on other issues of tsunamis such as geophysical surveys (e.g., GPR and seismic profiling), tsunami waveform modeling, sediment transport and flow speed modeling, sequences older than Holocene etc. are excluded. Among the 285 studies, 172 of them include sedimentary records of only “single event”. In other words, 68 papers are about the 2004 Sumatra tsunami, 25 papers about 2011 Tohoku tsunami, 14 papers are about the 1755 Transatlantic Lisbon tsunami. Twenty-eight studies are review papers. Among these, only 85 papers present paleotsunami chronologies.

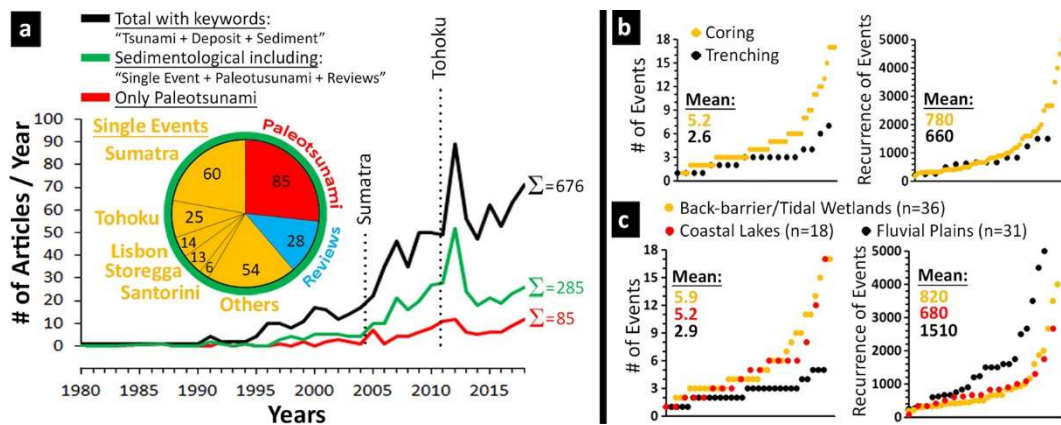


Figure 1.5 a) The number of papers per year in the “Web of Science” database; Black Line: all papers using the keywords of “Tsunami+Deposit+Sediment” (total of 676); Green Line: the papers of which main focus is sedimentological investigations (total of 285); Red Line: the papers presenting paleotsunami chronologies (total of 85). The “real” sedimentological studies (pie chart) comprise 172 papers focusing on the deposits of only “single events”, 85 paleotsunami papers, and 28 review papers. b) and c) Among the paleotsunami studies, comparison of papers on coring vs. trenching, and different depositional environments in terms of the number of detected tsunamis and their mean recurrences per study. The studies are sorted along the x-axis. (From Avşar, 2019b)

Evaluation of performances of coring versus trenching methods and the suitability of different depositional environments for paleotsunami research are depicted in Fig. 1.5b. Although these studies are from regions having different tsunamigenic tectonic settings, the number of paleotsunamis detected by coring methods are higher than the trenching methods (compare Fig 1.5b and c). However, there is no significant difference in the calculated recurrence of the events per study (Fig. 1.5b). This is probably because longer sedimentary sequences can be recovered and studied by coring (Avşar, 2019b). On the other hand, back-barrier/tidal wetlands and coastal lakes, where a generally higher number of events with lower recurrence intervals is found, seem to be more suitable environments than fluvial plains (Fig. 1.5c). The reason is that fluvial plains are more susceptible to natural and

anthropogenic erosive processes, which may cause significant stratigraphical hiatuses in sedimentary sequences.

The techniques used in paleotsunami studies utilise fingerprints of tsunamis on land such as variations in the spatial distribution and sedimentary facies analysis that includes composition, grain-size, packing, sorting, etc. (Sugawara et al., 2008; Avşar, 2019a). Explicitly, basal erosional unconformities, fining-upward and fining-landward, variation in the content of marine fossils, rip-up clasts from underlying units, and mud caps which are the most typical sedimentary features used in tsunami investigations (Röbke and Vött, 2017). When examining onshore paleotsunami studies, it is seen that poorly sorted, bimodal and fining upward sequence deposits are used to identify event deposits, which are deposited as a result of short-duration abnormal high-energy processes (Marriner et al., 2017). While in coring technique, it enables making grain-size analysis and biogenic-content analysis, in trenching technique, it gives chance to see succession.

Since tsunamis have the ability to transport material from sea to land, traces of this transportation can be investigated within the sedimentary sequences of nearshore depositional environments. For example, tsunamis are high energy events; the grain-size distribution of their deposits can be expected to be coarser. Besides, lagoons and coastal wetlands are brackish water environments, if the material is transported from the sea during the tsunami, intercalations of sediments containing marine species are found within brackish water species. In Figure 1.6, the bar chart of the number of papers using different “methods/analyses” in their sedimentological studies is provided. Obviously, the most commonly applied method is the grain-size distribution analysis (e.g. Nanayama et al., 2007; Smedile et al., 2011; Razjigaeva et al., 2014; Dura et al., 2015; Graehl et al., 2015), which provides valuable information about the hydrodynamic conditions during deposition; e.g., fining-upward sequences reflecting the decrease in the turbulence of the flow during inundation. Although there have been studies that applied loss-on-ignition, magnetic susceptibility and XRD mineralogy methods (e.g. Bertrand et

al., 2011; Dura et al., 2015; Kempf et al., 2017), these methods did not provide understandable information about tsunami deposits.

Micropaleontological analyses on diatoms (e.g. Kelsey et al., 2005; Goff et al., 2011; Dura et al., 2015; Graehl et al., 2015), foraminifera (e.g. Mamo et al., 2009; Bertrand et al., 2011; Pilarczyk and Reinhardt, 2012; Mathes-Schmidt et al., 2013; Willershauser et al., 2015; Fischer et al. 2016), Ostracoda (e.g. Ruiz et al. 2010; Mischke et al., 2012) and pollen (e.g., Hughes et al., 2002) assemblages in tsunami deposits are other commonly applied methods for discriminating marine versus terrigenous origin of deposits.

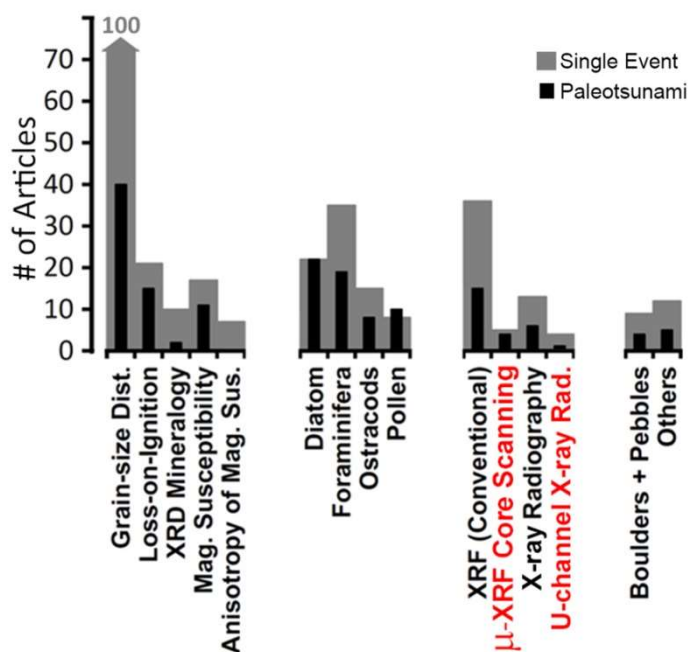


Figure 1.6. Different methods used in sedimentological investigations on tsunami deposits versus the number of papers used them. Note that high-resolution micro-XRF core scanning and u-channel X-ray radiography, the main techniques applied in this study, has not been used commonly.

Several studies have utilized conventional XRF analysis to trace chemical fingerprints of marine origin of tsunami deposits (e.g., Vött et al., 2009; 2011). In general, tsunami deposits are found to be enriched in elements like sodium,

sulphur, chlorine, calcium, strontium and magnesium; reflecting their marine origin. Although a reasonable amount of geochemical knowledge on tsunami deposits has been obtained by conventional XRF analysis, the use of high-resolution micro-XRF scanning is limited to only 5 “single event” studies and four paleotsunami studies (Figure 1.6).

Tsunami deposits also have some characteristic sedimentary structures, which were studied only by visual observations, such as sharp basal contact, scour-and-fill structures, rip-up clasts, the imbrication of shells, and cross-bedding etc. The u-channel radiography method, which uses thin sediment slabs rather than half core sections like in conventional radiography, is advantageous primarily if detailed sedimentary structures are targeted (e.g., Avşar et al., 2016). Conventional X-ray radiography has been used in 19 studies. However, the use of u-channel X-ray radiography has been much less. So far, only 4 “single event” studies used u-channel X-ray radiography, and it has never been used in any paleotsunami investigation.

To understand the recurrence of the tsunami disaster, investigations on this hazard needs to be deepened. If its frequency and recurrence are known, mitigation of tsunami risks can readily be taken before the event. Thus, environmentally, economic and survival risks will be minimized. In summary, based on the information presented in Figure 1.5 and 1.6, it is seen that high-resolution sedimentological investigations to be carried out in lagoons like Ölüdeniz can significantly improve our knowledge of past tsunamis.

1.3 Study Area

Ölüdeniz Lagoon is located in the southwestern part of Turkey (36.5522 N, 29.1102 E), in the eastern Mediterranean. The West Anatolia is geodynamically very active region. In the region, Hellenic (in the west) arc and Cyprus arc (in the east), 400 km offset from each other (Hall et al., 2014), dominates Mediterranean’s

structural formation. These arcs represent convergence of the African and Arabian plates with the Eurasian Plate, with the Aegean-Anatolian Microplate (McKenzie, 1972; Dewey and Şengör, 1979; Dewey et al., 1986; Le Pichon and Kreemer, 2010). As a result of differential motion of these arcs, a Subduction Transform Edge Propagator ('STEP') fault zone (Govers and Wortel, 2005) has appeared along the transfer zone where these two arcs connected to each other. Ptolemy, Pliny and Strabo trenches are the most conspicuous structure related with STEP fault (Hall et al., 2014). These trenches identify 50 km wide fault zone (Özbakır et al., 2013). Ocakoğlu (2012) found fault linkages of Pliny-Strabo trench to the Fethiye-Burdur fault zone, passing through Fethiye Bay. From this view, Ölüdeniz lagoon is in an ideal geographical setting that could prone to tsunamis in the eastern Mediterranean (Figure 1.7 and 2.1). Despite being very near to Fethiye Bay, tsunamis in Ölüdeniz region is not related to Fethiye-Burdur fault zone. Generally, tsunamigenic earthquakes are mostly produced by Pliny-Strabo trenches in the region.

The study area finds itself in the west Anatolia having very complex fault system and different tectonic characteristics in Neogene basins, which are separated into different basins depending on the similarity of tectonic characteristics, such as Çameli basin and Acıpayam basin (Kaymakci et al., 2018). The study area is composed of Lycian nappe units and quaternary alluvial, located in the Eşen basin. (Figure 1.7a). In the close vicinity, there is only Eşen fault as an active fault within 40 km (Figure 1.7b). However, there is on paleoseismological records related with this fault. There is only one earthquake instrumentally recorded, which may be related with this fault, happened in 1968, Mw=4.8 (Figure 1.8a).

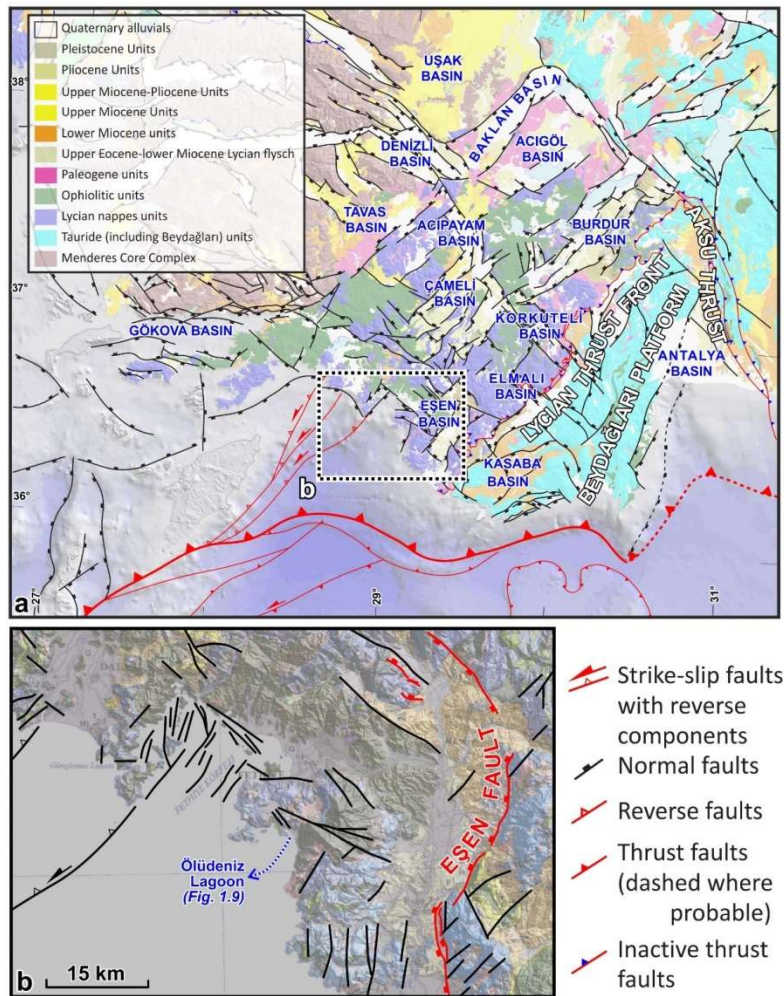


Figure 1.7. a) Geological units and active fault systems around the study area, SW Turkey (Kaymacı et al., 2018), b) Fault types near the vicinity of Ölüdeniz lagoon within about 40 km (MTA, 1997 ,1/250000 Scale Geological Maps of Turkey, No:2 Fethiye; Emre et al., 2018; Tosun, 2018)

Considering the period between 1900 and 2020, there has been no strong earthquake around the lagoon. During these 120 years, the highest peak ground acceleration (PGA) at the lagoon was due to an earthquake at ca. 20 km to the southwest of the lagoon with a magnitude of 6.0 in 2012 (Figure 1.8a). The PGA due to this earthquake is estimated at around 50 cm/s² by using the attenuation relationship by Akkar and Çağnan (2010). The lagoon is isolated from the Mediterranean Sea by a ca. 500-m-long sand spit, the elevation of which does not

exceed 5 m a.s.l. (Figure 1.8b). The width of the sand spit mostly does not exceed 150 m, which would easily allow overwash during tsunamis. Hence, the material ripped up from the nearshore and sand spit as well by overwashing water could easily be transported into the lagoon and be deposited as intercalations within the background sedimentation (Avşar, 2019a). According to Şenel (1997), a significant proportion of Ölüdeniz catchment is limestone (Figure 1.8b).

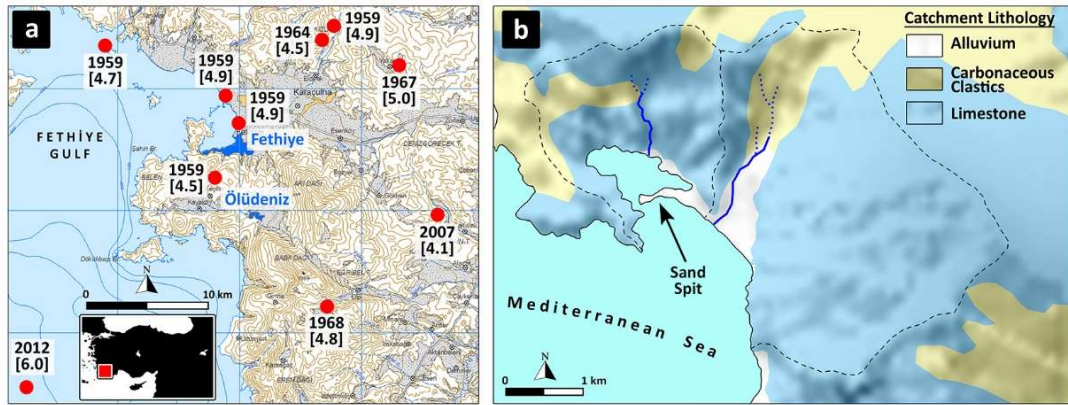


Figure 1.8. a) Active fault map around Ölüdeniz Lagoon Emre et al. (2011). Instrumentally recorded earthquakes ($M_w \geq 4$) around the lagoon during 1900–2020 are also shown (KOERI-NEMC EQ Catalog - <http://www.koeri.boun.edu.tr>). b) Close-up view to the catchment of Ölüdeniz Lagoon and the lithology on relief-shaded map (Şenel, 1997)

1.4 Methods

1.4.1 Bathymetric Map

Before all coring operations in aqueous environments, bathymetric surveys should be carried out in order to reveal basin geometry and avoid coring on basin slopes, where sedimentation may not be continuous. Bathymetric map of Ölüdeniz Lagoon was obtained by using “JEOLODTÜ” sediment coring platform of Geological Engineering Department of METU (Figure 1.9a), which is equipped with a sonar-mounted Global Positioning System (GPS) instrument (Garmin GPS map 421s).

Water depth was measured every 5 seconds along the routes shown in Figure 1.9b, while the platform was cruising at an approximate speed of 7-7.5 km/h, which roughly corresponds to measurements at every 2 m. The data were then interpolated in MapInfo Software to obtain the bathymetric map (Figure 1.9c). This map is prepared for planning investigation and determining borehole locations.

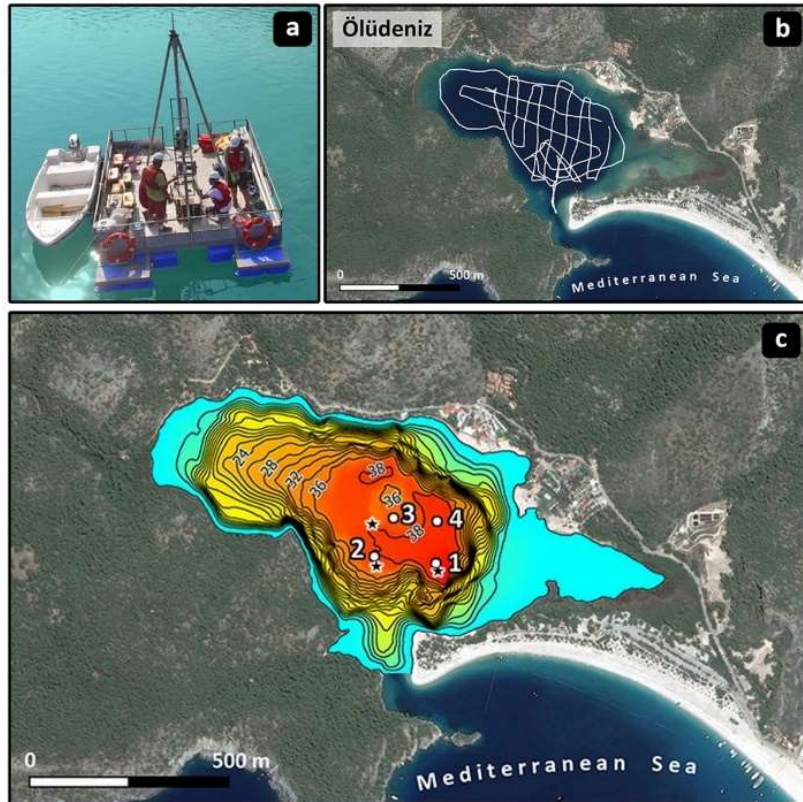


Figure 1.9. a) Sediment coring platform JEOLDTÜ. b) The route followed for bathymetric measurements. c) Bathymetric map of Ölüdeniz Lagoon and coring locations. While stars represent coring locations of Avşar (2019a), white dots represent coring locations of this study.

1.4.2 Piston Coring

There are many types of coring techniques to obtain and make investigations on sedimentary sequences. Gouge Auger, Russian peat corer, piston corer, Mackereth corer are good examples for sampling techniques. Amongst others, piston corer is

an easy and efficient sampling method in aquatic environments to obtain undisturbed sediment cores. Basically, it is designed to work in a saturated environment with minimum or no disturbance on sampling, and this technique is based on Kullenberg design (Emery and Broussard, 1954).

Composition of piston coring and processes are schematized in Figure 1.10-1 (Avşar, 2013): (a) core catcher, (b) piston, (c) PVC liner, (d) anvil, (e) doughnut hammer, and (f) guide rod. The core catcher is used for holding and preserving sample in the tube while taking it back so that we do not lose any sample from the tube and not to disrupt the integrity of the sequence. The piston is used to create the vacuum in the pipe needed during penetration so that the friction between the sediment and the pipe would not push the sediments down during penetration. The PVC pipe is tightly attached to the anvil, on which the hammer hits during operation.

Before starting the operation, the platform is fixed at the coring location by anchoring from three directions, and water depth is precisely measured. Then, the whole system is slowly lowered until the catcher gets as close as possible to the bottom (Figure 1.10-2). During the whole lowering operation, the key point is that the hammering and piston ropes should always be loose. Especially if the piston rope gets tight even for a few seconds, it will pull and slide the piston up in the pipe before we start hammering, which results in a core shorter than the full pipe length. After getting reached to the bottom, piston rope needs to be locked, and the main rope should be slightly tensioned so that the whole system can be kept vertical, but moves down at each hit of hammering (Figure 1.10-2). During hammering, PVC liner penetrates into sediments, but the piston does not move, which creates the required vacuum (Figure 1.10-3). It is important that, as the hammering continues, piston rope should always be tight along whole processes to be sure the vacuum is continuous. If it gets loose, there may be a loss of vacuum; thus, it may cause taking discontinuous sediment and artificial sediment deformations. This is why piston coring should always be done during totally stagnant water conditions; otherwise, waves move the platform up and down that prevents us from giving

continuous tension on main and piston ropes. Samples taken during rough water conditions are not undisturbed sediment cores; they are just mud in the pipe. After getting reached to the desired depth (Figure 1.10-4), the system should be strongly pulled by both main and piston ropes to be able to rip it from the sediments (Figure 1.10-5). While taking it back, the core catcher will be closed and not allow the sediments to slide down from the pipe. Since the operation is done, there is no need to hold piston rope tightly. The whole system is pulled back to the platform.

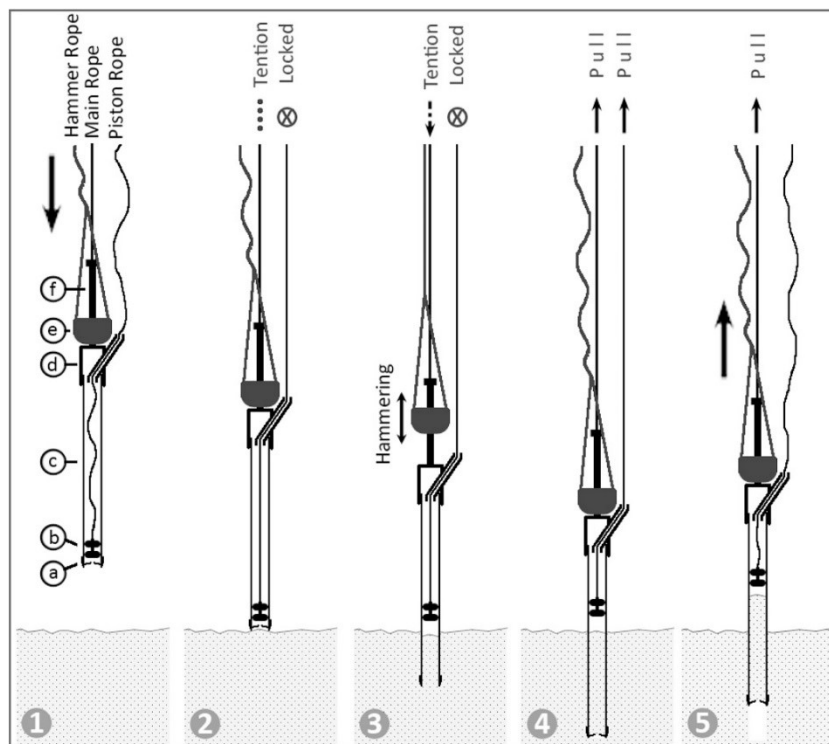


Figure 1.10. Schematized steps of piston coring operation (Avşar, 2013)

Coring locations were decided based on the bathymetric map. Selected locations are on the flattest and deepest part of the lagoon. The slopes of basins are avoided because of two main reasons: 1) occasional slope failures (slump, etc.) would create hiatus in the sedimentary record, and 2) sedimentation rate close to the edges of basins is always higher compared to the middle parts, which results in shorter records in terms of time with same core lengths. Coordinates, depths and lengths of the cores taken from Ölüdeniz Lagoon in summer 2017 are listed in Table 1.3.

Table 1.3 Brief information on the cores taken from Ölüdeniz Lagoon

Core ID	Coordinates		Core Length (cm)	Water Depth (m)
	X	Y		
OLD-1	688972	4047213	305	38.5
OLD-2	688815	4047221	367	37.6
OLD-4	688970	4047317	370	38.5

For laboratory analyses, they need to be prepared. Thus, after getting the cores, they were sent to Ankara for preparation under very well-preserved condition. Here, they were separated into two halves and protected in the cold room until sending for laboratory analyses.

1.4.3 ITRAX micro-XRF Core Scanning

After coring operations, the cores were sent to Ankara for splitting and extraction of u-channels that would be scanned by ITRAX micro-XRF scanner. ITRAX basically provides three types of data: 1) RGB high-resolution optical images, 2) Radiographic images, and 3) high-resolution X-Ray Fluorescence (XRF) data (down to 0.2 mm increments). In this study, the first step was to extract u-channels from the split cores in Ankara, and then u-channels were sent to GEOPOLAR Laboratory of Bremen University for ITRAX scans.

ITRAX analysis is a widely used technique in paleoenvironmental studies. The change in environmental conditions can easily be differentiated by looking at changes in the physical and geochemical properties of sediments along the cores. ITRAX is more effective than the traditional XRF measurements in terms of speed of getting data and analysis costs. The components of the ITRAX system are schematized in Figure 1.11a. The split-core is put on the tray of the device, which slides under the sensors during measurements. The system operates in 4 steps: 1) It firstly produces the RGB image of the core by using its optical line-scan camera (A, Figure 1.11a). 2) Radiographic image is obtained. X-rays produced by the source (D) pass through the flat-beam waveguide (E) that produces 0.1 mm thick and 2 cm wide beam. Then, the beam pass through the sediments and the number

of successful x-rays is recorded by X-ray line-scan camera (F). 3) Before XRF scanning, the system precisely measures the surface topography of the core along the measurement line by its triangular laser system (B), so that the motorized XRF detector (C) adjusts its distance to the core during XRF scanning. 4) Finally, XRF scanning is done at increments decided by the user (down to 0.2 mm increments).

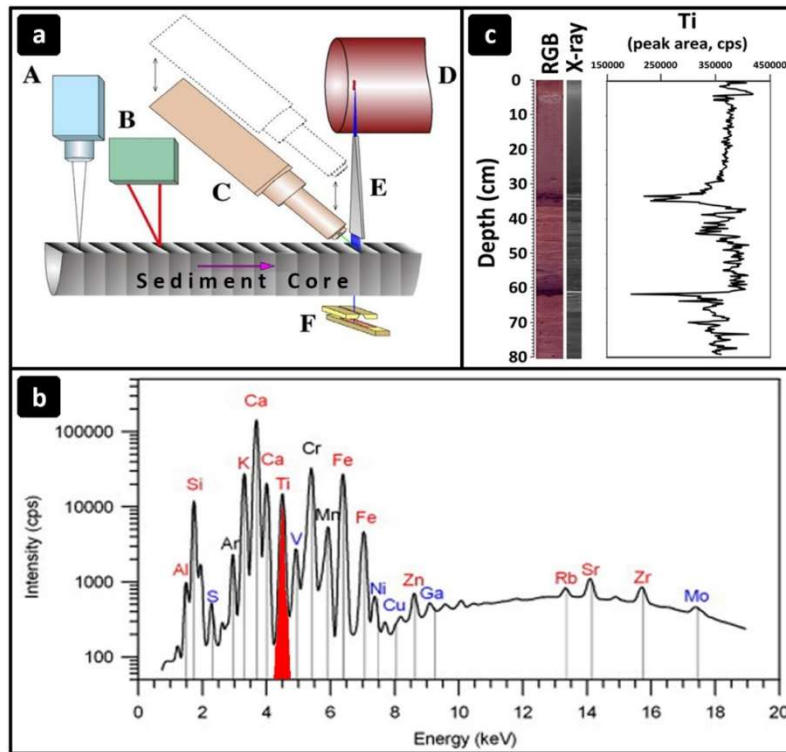


Figure 1.11. Principles of ITRAX micro-XRF core scanning, (a) Components of ITRAX micro-XRF system (Croudace et al., 2006). A: optical line-scan camera, B: triangular laser system, C: motorized XRF Si-drift chamber detector, D: 3 kW X-ray tube, E: flat-beam X-ray waveguide, and F: The X-ray line camera. (b) A typical XRF spectrum produced by ITRAX (from Liang et al., 2012). (c) Example of RGB image, radiograph and Ti profile produced by ITRAX (from Boraboy Lake, Avşar et al., 2015).

During XRF scanning, ITRAX produces XRF spectra for each measurement point. A spectrum is a plot of incident X-ray energy (keV) versus detected intensity of photon emission from the sample (cps). Elements have specific levels of incident

X-ray energy to emit photons, which appear on XRF spectra as peaks. For example (Figure 1.11b), Ti emits photons when the X-ray energy is around 4.5 keV, and the rate of emission (i.e. the height of the peak) is a function of the concentration of Ti in the sample. After scanning is completed, ITRAX software investigates each spectrum one by one and detects peaks, and calculates their areas. In Figure 1.11c, outputs of ITRAX are illustrated for the gravity core from Boraboy Lake (Amasya/Turkey); RGB optical image (6.6 cm wide), radiographic image (2 cm wide), and Ti profile measured at every 2 mm (Avşar, 2013; Avşar et al. 2015).

Radiographic images are used to understand primary/secondary sedimentary structures, as well as density changes along the cores. It is a very useful tool to understand soft-sediment deformations and inclinations (e.g. Migeon et al., 1999; Avşar et al., 2016). Denser materials attenuate X-rays more; hence X-ray line-scan camera under the core detects less X-rays. Thus, denser sediments appear darker in radiographic images. In addition to sedimentary structure observations, grayscale profiles of radiographic images are used to evaluate variations in bulk density along cores. Fine-grained sediments are more easily compacted than coarse grains. Accordingly, the weight for a cm³ increases at these levels, i.e., these levels become denser. Hence, these fine-grained levels seem darker in radiographic images.

U-channel extraction is vital to observe sedimentary structures better. If the core does not contain perfectly horizontal and planar layers (or laminations), the radiographic images obtained through half-cores (generally 5-6 cm in radius) are generally blurred. Since u-channel radiography is done along thin slices of sediments (1-2 cm-thick), images obtained show sedimentary structures much better. Figure 1.12a and b illustrate the comparison of half-core and u-channel radiographies of cores from Boraboy Lake (Turkey, Avşar et al., 2015) and Hoskuldsvatn Lake (Iceland, Avşar et al., 2013), respectively. As it is clearly seen, u-channel radiography shows much more details. Especially on the core from Hoskuldsvatn Lake, the deformation due to coring, which can even be seen by the unaided eye on the RGB image of the core, is not observed in the half-core

radiography, while u-channel radiography clearly reveals the deformation (Figure 1.12b). Figure 1.12c illustrates the steps during u-channel extraction: 1) PVC u-channel is put on the surface of split-core, 2) It is gently pushed into the sediments until fully filled, 3) Sediments at both sides of the u-channel are removed (Figure 1.12d), and finally 4) Sediments are cut by using fish line and u-channel is extracted.

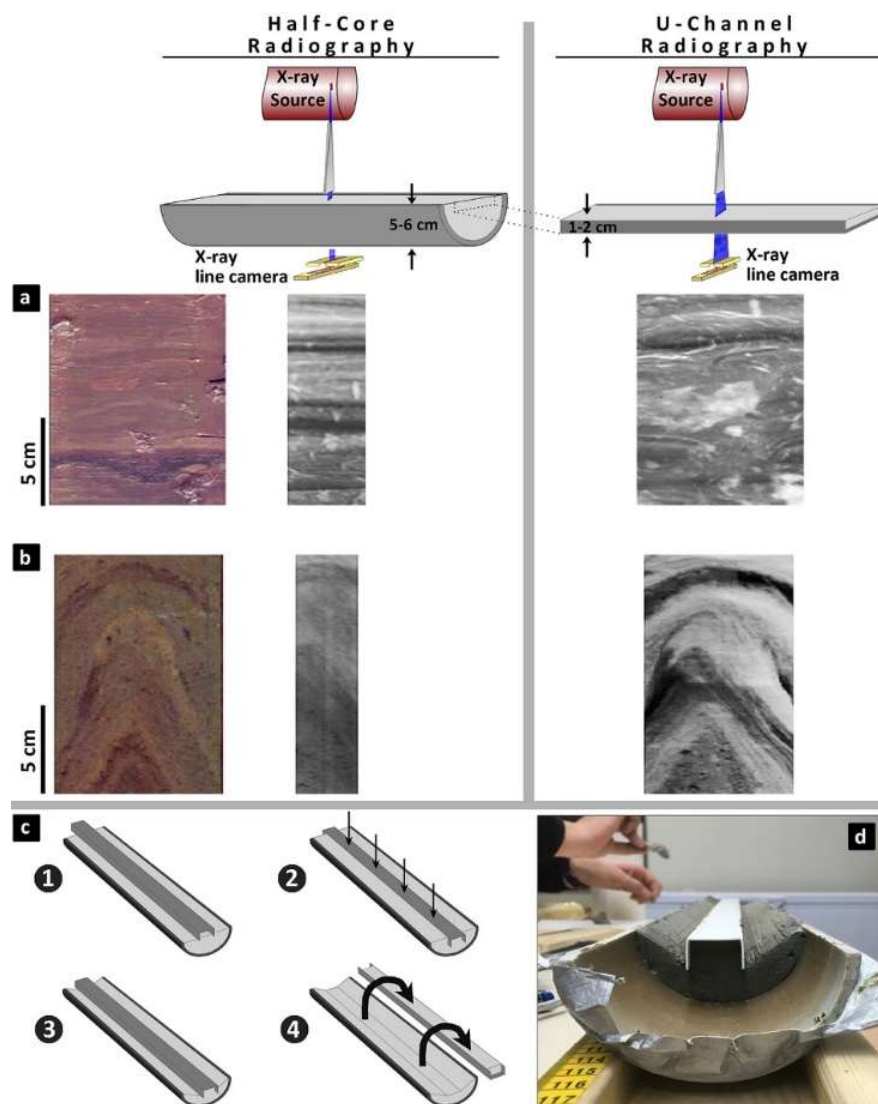


Figure 1.12. a) and b) Comparison of half-core and u-channel radiographies. c) Schematic illustration of steps to extract u-channels from split-cores. d) View of a split-core after sediments on both sides of the u-channel were removed. “c” and “d” are from Avşar (2019b).

Prepared u-channel samples are sent for laboratory analyses to GEOPOLAR Laboratory, Bremen University, Germany. Here, ITRAX micro-XRF core scanning method was applied on the samples to search elemental ratio and to get optical and radiographic images of samples. Although giving semi-quantitative results in contrast to conventional XRF analysis, this technique provides higher resolution and faster results. While conventional XRF technique spends about 2 weeks for a 1-m core at 1 cm increments, ITRAX micro-XRF core scanner can handle with the same work just in a few hours, in 200 μm increments (Croudace et al., 2006).

In the ITRAX micro-XRF scanning, there are two X-ray source tubes used widely, Molybdenum (Mo) and Chromium (Cr). While Mo works more efficient for heavier elements ($Z > \text{Fe}$), Cr works more efficient in lighter elements ($Z < \text{Fe}$) (Croudace et al., 2006). However, within the scope of the study, we need more data. Thus Mo-tube was used in our study because it gives a wider range of elements at the end of the experiment. Our ITRAX analysis was executed in GEOPOLAR Laboratory at the University of Bremen. We took optical and radiographic images in 0.2 mm resolution and applied XRF analysis at 1 mm increments. All these analyses were applied to u-channels. During XRF analysis, dwell time was 5 seconds in each 1 mm increment.

Acquired data from XRF scanning show differences in terms of quantity of constituents. For example, while mean values of Ca profiles are around 100000 counts per second (cps), Cu show approximately 200 cps. At this level, these elements are not comparable. So as to bring all these on a comparable level, they need to be standardized. For each element, we need to estimate the mean (μ) and standard deviation (σ) values to acquire standardized values, which were calculated by the following equation;

$$z = \frac{x - \mu}{\sigma}$$

Where,

x = Data Value, μ = Mean Value, and σ = Standard Deviation

Following data standardization, these standardized data are also used in inter-element ratios, which are used to estimate the ratio of deposited sediment at a certain level; i.e., we can determine the concentration of each element with respect to each other. If any sudden change exists along the inter-element ratio curve created for the whole sample, we can suspect about this change as a sedimentary event reflecting a geological impact. Especially, in our study, if there was a tsunami in the past, these tsunami-waves would transport terrigenous elements from the sand-spit of Ölüdeniz Lagoon. Then, these wave-borne sediments would be deposited in the lagoon. In our inter-element ratio, we must see sudden change along the curve because there will be a terrigenous impact in the lagoon due to tsunami. In this context, Ti/Ca ratios from XRF data are used to understand the tsunami impact since Ti is one of the ninth most abundant elements on earth surface (Clarke and Washington, 1924; Darling, 2007). Sudden deposition of terrigenous sediments proportionally increases the Ti concentrations. Since chemical or biogenic Ca precipitation from the water column is slower during a sudden event, Ti/Ca ratio profile is expected to show significant peaks in tsunami deposits intercalated with lagoon sediment.

1.4.4 Radiocarbon Dating

In paleotsunami research, in order to provide age control on the events, we need to date the sediments. There are many types of radiometric methods. Uranium-series dating techniques, optically stimulated luminescence, cosmogenic isotope dating and radiocarbon dating are the most commonly used ones. In our study, since organic material is available along the cores, the radiocarbon dating technique was preferred amongst others. This technique is based on the decay counting of ^{14}C in organic tissues (Björck and Wohlfarth, 2002). ^{14}C is continuously produced in the upper atmosphere, where it is rapidly oxidized and produces C^{14}O_2 . This CO_2 is used by organisms in forming their tissue, and following the organisms' death, CO_2 intake into the tissue stops. Then, ^{14}C in the organism starts to decay (Björck and

Wohlfarth, 2002). Age measurements of fossil organic matter are based on this decay, which is based on internationally agreed and fixed half-life value for ^{14}C as 5568 years (Mook, 1986). However, because of combustion of fossil fuels (producing old CO_2) and nuclear weapon tests (increased ^{14}C production) (Björck and Wohlfarth, 2002), estimated values may not be useful for the last two hundred years, thus, such short intervals may be dated by short-lived ^{210}Pb and ^{137}Cs radioisotopes and complement ^{14}C method (Björck & Wohlfarth, 2002). As it is in almost all experiments, in radiocarbon dating technique, there are also errors sourced by; instrumentally, hard water/reservoir effect and/or contamination of young and old materials (reworking and deposition of older organic deposits, infiltration of humic acid, root penetration, bioturbation) (Björck & Wohlfarth, 2002). Allochthonous organic matter, transported with any agent to the lake may cause great variation in measurements. It may belong to older organisms, and in the estimation of age may cause overestimation. For younger age estimations related to contamination may be sourced by roots penetrating into the sediments, from infiltration by younger humic acids or through bioturbation (Olsson, 1991).

In aquatic environments, radiocarbon dating can be applied in C exists in CaCO_3 (e.g. bivalve shells) and/or transported terrigenous organic matters (e.g. tree leaves). However, CaCO_3 may be subjected to a reservoir and/or hard water effect during its existence in the water. CaCO_3 in the water used by organisms (mollusk shells and/or aquatic plants) may come from CaCO_3 deposited millions of years ago, such as from Cretaceous limestone. This may cause overestimation on getting results. ^{14}C , used in dating, may also be subjected to reservoir effect which means if $^{14}\text{C}/^{12}\text{C}$ of tissue of an organism is lower than the lake; it will cause great changes in radiocarbon dating, as well. This discrepancy is generally caused by the influence of glacial melt-water (Björck and Wohlfarth, 2002). Contrary to aquatic Carbon sources, terrigenous organic matter does not include such effects. According to Shotton (1972), if there is tree wood or leaves, twigs or seeds of wholly terrigenous plants, there will not be a hard water effect. Thus, if terrigenous organic matter exists along a core, it would be the best option for radiocarbon

dating. Dating can easily be estimated by using the ratio of unstable ^{14}C element to stable ^{13}C and ^{12}C without considering any effect because these carbons will be in equilibrium with the atmosphere so the terrigenous organic matter will be more trustable. Calibration of all raw radiocarbon dates in this study was done by OxCal software (Bronk Ramsey, 2017) using IntCal13 atmospheric curve of Reimer et al. (2013).

1.4.5 Temporal Correlation with Historical Records

From the principle of Uniformitarianism, “Present is key to the past”, current geological processes shed light on the ancient ones. In paleotsunami investigation, current tsunami traces are helping to understand past events. These investigations are conducted in several ways such as geophysical, geological, geomorphological and archaeological. However, since storm deposits/traces show similarity with tsunamigenic ones, there may impose confusion in the interpretation of revealed sedimentary events. At this time, when sedimentary events revealed with the methods mentioned above are temporally correlated with historic tsunami records, tsunamis become “usual suspects” responsible for these sedimentary events. Thus, historical records have an important place in paleotsunami investigations. For example, Ibn-i Hajar mentions:

'On 10 Sha'ban 811 [29 December 1408] a great earthquake affected the districts belonging to Aleppo and Tripoli, and destroyed a number of places in Latakia, ... The shock also affected Cyprus, where many places were destroyed in the mountains and the plains [lit. "watering places"}. Snow was seen on the top of Jabal Aqra' [Jebel Akra, 1759 m], and the sea receded for 10 farsakhs [about 60 km, sic.] and then returned. Ships at sea touched the bottom before the water returned to normal, without hurting anyone.' (Ambraseys, 2009)

From this perspective, historical records are very helpful in order to raise the correctness rate (reliability) of our paleotsunami studies. Since the Mediterranean region has served as home for many civilizations and it is one of the oldest places where people live, it has many historically recorded events. In the light of consistency between historical records and sedimentary events detected, it is possible and reasonable that similar sedimentary events found at the deeper parts of the sedimentary sequence can also be interpreted as tsunamis. In this way, we can also have information about tsunamis of pre-historical times. This enables us to add remarkable contributions to our and international paleotsunami investigations, especially learning about intensity and recurrence intervals of tsunamis in the Mediterranean region for public safety.

CHAPTER 2

LITERATURE REVIEW

2.1 The Eastern Mediterranean Tsunamis

Since a few decades ago, the general opinion about tsunamis was to occur mostly in the Pacific region. Mediterranean region had not been thought for this disaster to occur, or it was thought to be rare. However, Hellenic Arc, dominating the eastern Mediterranean, is geodynamical very active due to lithospheric plate convergence, which results in high seismicity and volcanism in the region (Papadopoulos, 2016).

Based on the historical records, Gusiakov (2009) states that there has been 2100 tsunamis and tsunami-like events during the last 4000 years, of which 26 (545) occurred in the Mediterranean region. Although there are several different tsunami catalogues and tsunami intensity scales that could be used for the tsunamis worldwide, the intensity scale prepared by Papadopoulos and Imamura (2001) is especially suitable for the eastern Mediterranean because it was designed by considering the historical structure and resource quality of the region. According to this 12-grade intensity scale, Papadopoulos et al. (2014) reports that, in the Mediterranean and the connected seas, there have been 44 tsunamis having intensities higher 6 (Table 2.1), which means wave-height was more than 2 m, and they were stronger than “slightly damaging”.

Table 2.1 Historically known strong tsunamis (having intensities higher than 6) in the Mediterranean and connected seas (Papadopoulos et al., 2014). The ones having the potential to be felt around Ölüdeniz Lagoon are highlighted.

No	Year	Month	Day	Region	Area/K	<i>h</i> (cm)	ML
1	-426	Summer		Maliac Bay	8		
2	-373	Winter		W. Corinth Gulf	Helike 9		
3	148			Rhodes Isl.	Rhodes 7		
4	365	07	21	Crete Isl.	Alexandria 10		
5	447	01	26	Marmara Sea	8		
6	544			Bulgarian Black Sea	8-9		
7	551	07	09	Lebanon	8		
8	556			Cos Isl.	Cos 8		
9	749	01	18	Levantine coast	7		
10	1169	02	04	Messina Straits	8		
11	1202	05	20	Syrian cost & Cyprus	7		
12	1303	08	08	Crete Isl.	Heraklion 10		
13	1343	10	18	Marmara Sea	8	200	
14	1365	01	02	Algiers	8		
15	1389	03	20	Chios Isl.	6		
16	1402	06		Corinth Gulf	8		
17	1481	05	03	Rhodes Isl.	Rhodes 7		
18	1598	05		Turkish Black Sea	8-9		
19	1609	04		Rhodes Isl.	Rhodes 8		
20	1627	07	30	Gargano	6		-1.4
21	1650	10	11	Thera Isl.	Patmos 10	2000	+3.0
22	1693	01	11	Eastern Sicily	7		+2.3
23	1741	01	31	Rhodes Isl.	Rhodes 8		
24	1748	05	25	W. Corinth Gulf	Aeghion 9	1000	
25	1755	11	01	SW Iberia	Lisbon 10	1500	+3.8
26	1759	11	25	Levantine Sea	Akko 8		
27	1766	05	22	Marmara Sea	7		
28	1773	05	06	Tangiers	7	900	
29	1783	02	06	Calabria	9	900	-1.8
30	1817	08	23	W. Corinth Gulf	Aeghion 9	500	
31	1823	03	05	North Sicily	8		
32	1856	11	13	Chios Isl.	8		
33	1866	01	02	Albania	7		
34	1866	02	02	Kythira Isl.	Avlemonas 6	800	
35	1866	03	06	Albania	7		
36	1867	09	09	SE Peloponnese	Gythion 7		
37	1908	12	28	Messina Straits	10	1300	-0.4
38	1944	08	20	Stromboli Isl.	7		
39	1948	02	09	Karpathos Isl.	7		
40	1956	07	09	Cyclades	Astypalaea 9	1500	+3.0
41	1963	02	07	W. Corinth Gulf	7	500	-11.0
42	1979	04	15	Montenegro	8		
43	1999	08	17	Marmara Sea	6	250	
44	2002	12	30	Stromboli Isl.	Ficogrande 7	900	

Among 44 tsunamis listed in Table 2.1, eleven seem to have potential to be felt all along the eastern Mediterranean, and around Ölüdeniz Lagoon as well. Papadopoulos et al. (2014) also provide the approximate epicentral locations of the earthquakes triggered these tsunamis (Figure 1.7, red stars). In addition, Salamon et al. (2007) report past tsunamis along with the eastern coast of the Mediterranean Sea during the last 2500 years. These two studies were taken as the basis of historical tsunami records for this study. For the eastern Mediterranean, Hellenic Arc, Cyprus Arc and the Dead Sea Transform Fault are the primary tectonic tsunamigenic sources (Figure 1.7). Their potential to trigger tsunamis are determined as “high” for the eastern Hellenic Arc, “intermediate” for the Dead Sea Fault, and “low” for Cyprus Arc (Yolsal et al., 2007; Papadopoulos et al., 2014).

2.2 Previous Studies

In addition to the historical records, geological traces of past tsunamis have been investigated at 16 locations around the eastern Mediterranean (Figure 2.1, yellow diamonds). Although the details about these studies are given in the following parts of this section, it can be briefly said that studies providing paleotsunami chronologies, i.e. including several succeeding tsunami deposits, are highly limited in the region. The paleotsunami records detected at Didim (Di; Minoura et al., 2000), Fethiye (F; Minoura et al., 2000) and East Crete (EC; Bruins et al. 2008) are the traces of only Santorini Tsunami that was around 1613 BCE. Similarly, single events also detected in the sequences of Kefr Saber (KS, Egypt) in CE 365, Alexandria (Al, Egypt) in CE 1303, Ashkelon (As, Israel) around 400 BCE, Crete (WC-2) in CE 365, Marsa-Matrouh (Ma, Egypt) CE 1303, Cyprus (Cy1-Cy-2) CE 1500-1800, and Silifke (Si, Turkey) in CE 1953. Among 16 localities, multiple events that could help to understand recurrence of tsunamis have been found only at 6 locations; Caesarea (Ca, Israel), Dalaman (D, Turkey), El Alamein (EA, Egypt), Lebanon (Le), West Crete (WC-1), and Ölüdeniz (Ö, Turkey). In the

following pages of this section, findings of these studies are summarized in order of date of tsunami around the eastern Mediterranean.



Figure 2.1. Possible tectonic tsunami sources (Hellenic Arc, Cyprus Arc, Pliny & Strabo trenches and Dead Sea Fault; simplified from Barka and Reilinger, 1997), historical tsunamis (from Salamon et al., 2007 and Papadopoulos et al., 2014), and study sites of geological records of past tsunamis in the Eastern Mediterranean. Ölüdeniz Lagoon is well located to evaluate past tsunamis in the eastern Mediterranean.

Pirazzoli et al. (1992) opened three geoarchaeological trenches, A, B and C in an archaeological site called Phalasarna, which is a small port located in the west coast of Crete (Figure 2.1, WC-1). In the light of previous studies about relative mean sea level changes in Phalasarna (Thommeret et al., 1981; Pirazzoli et al., 1981; 1982), Pirazzoli et al. (1992) investigated current geoarchaeological trenches from a geological perspective. According to other studies, there were 6 mean sea-level changes during the last few thousand years. Considering these, they tried to understand relative sea-level changes and their relationships with tectonic movements by using sediments deposited in the ancient harbor. Two of 6 sea-level changes pointed out historical tsunamis. While they saw tsunami deposits at two levels in trench A, one level in trench B, location of trench C seemed not affected by any tsunami. The lower level corresponds to 66 CE Tsunami, which is reported in numerous historical resources. At this deposition level, there is a sudden increase in siliciclastics and sudden decrease in carbonate materials. Irregular blocks with siliciclastic materials which are thought to be transported by “backwash” suggest a tsunami. This deposition was very limited on Phalasarna and not seen in other trenches. Thus Pirazzoli et al. (1992) think that the younger event seen in this trench was stronger than 66 CE tsunami. Similar stratigraphy exists in the second level, as well. This level was dated to 341-439 CE, most probably pointing out 365 CE tsunami.

Minoura et al. (2000), i.e. Di and F in Figure 2.1, started a search to find Santorini Tsunami deposits (ca. 1613 BCE) along Aegean coasts. They found sedimentary traces on some archaeological sites on the coast of Crete. However, since they have thought the event and its effective area are not well understood, this study was preceded in Turkey. They established a simulation model. Accordingly, the highest wave amplitude triggered by the collapse of Thera caldera is estimated to be 21 m on Ios Island. In the Western part of Turkey, this number is around 5 m. By using the trenching method, they investigated traces of tsunami inundation on the coasts of Didim and Fethiye, western Turkey. The study sites have not been subjected to any human activities since the Hellenic period. General stratigraphy of the sites

consists of fine to medium sand grains with marine fossils and non-marine sediments of coastal sequences. The sand layers were fining towards the inland. There was not a certain aspect or structure within the sand layers, indicating rapid deposition. In Didim trench, there is a 10-15 cm-thick yellowish-white layer of felsic tephra overlying fine sand layer containing carbonate grains. Since there is no erosional contact between the tephra and the underlying sand layer, it is understood that volcanic ash settled just after the deposition of sandy marine deposits. In the area, there is also silty mud that is rich in fossils of shallow-marine benthic foraminifera, which turn gradually into non-marine mud towards the inland. Similarly in Fethiye trench, siliciclastic grains underlie 5-10 cm-thick felsic tephra. Below this siliciclastic layer, there is non-marine sandy silt rich in plant debris and fragments of shallow-marine gastropods of the indeterminate genus. Furthermore, in Gouves archaeological site, they found a late Minoan potter's workshop that is covered by a thin layer of carbonate-rich sand and an underlying 10-20 cm-thick pumice layer. Unsorted grains of skeletal fragments in this carbonate sand layer imply marine inundation. This site is located 30-90 m inland and 2-3 m a.s.l. Thus, they interpreted that this site was inundated during the Santorini Tsunami. Refractive index values of tephra and pumice found in Didim and Gouves, respectively, shows that they are of Santorini origin. On the other hand, tephra in Fethiye was subjected to burial diagenesis and a little bit altered. According to radiocarbon dating data, the events in Didim and Fethiye have a temporal difference about 600 years which probably due to the mixing of older shell fragments with the sand. Eventually, Minoura et al. (2000) concluded that the sedimentation of marine materials in their studies was probably caused by the inundation of tsunami waves triggered by the volcanic event in late Minoan time, i.e. Santorini Tsunami in ca. 1613 BCE.

Whelan and Kelletat (2002) used geomorphic traces for tsunami events in two different sites in Cyprus; along the coasts of Paphos in the west Cyprus and Cape Greco in the east (Figure 2.1, Cy1 and Cy2, respectively). In the study, they showed boulders and boulder ridges located 5-10 m above a.s.l. and extended up to

15 m inland. These boulders, in variable weight from 1 to 55 tons, are separated from the present supra-littoral area. The presence of these boulders gives a significant clue about the tsunamigenic process. Besides, cobble and boulder terraces at Agios Theodoros near Cape Greco, cover 200-250 m-wide area above 3-3.5 m a.s.l., which present another trace for tsunamis. They think that these deposits are located far beyond storm waves can reach, and this can only be explained by tsunamigenic processes. Destructed cliffs and notches due to tsunami waves and bare rock platform stripped off any soil and vegetation, such as bare Aeolianite platform located on the western Akamas Peninsula 13 m a.s.l., are the other significant tsunami traces. They conclude that the geomorphic traces they detected should have been formed between CE 1530 and 1800.

Morhange et al. (2006) studied mega blocks lying on Tripoli islands and Byblos, in northern Lebanon (Figure 2.1, Le), which are thought to have been transported by extremely high-energy waves. In this region, there is an active thrust system, moving eastward and causes Mt. Lebanon to grow. In the last 3000 thousand years, this area has shown three major uplifts in 3000 BP, in the 6th century and possibly during the 10-11th centuries (Pirazzoli, 2005). They reviewed these vertical movements and correlated with these blocks. These blocks were covered by *Dendropoma* and calcareous algae on which radiocarbon dating was applied. When they dated to these blocks, they estimated the blocks on the Ile du Palmier as 5155 ± 40 C14 BP years, the blocks nearby island of Senani as 525 ± 40 BP, the blocks at Byblos as 855 ± 30 BP, and the conglomerate block as 710 ± 30 BP. On the basis of these results, radiocarbon data obtained from mega blocks in different sites of the coasts do not coincide with uplifting dates. Thus, they interpreted the source of these mega blocks for other different tsunamigenic processes.

Stanley and Bernasconi (2006) studied Holocene sediments deposited on Alexandria's Eastern Harbor and its evolution (Figure 2.1, Al). In this manner, they extracted 7 vibrocores with a 10-cm diameter at harbour depths ranging from 2.7 to 6.5 m and applied visual examination, photography, and X-ray radiography for each core. These core stratigraphies are formed with marine deposits, and

molluscan fauna is identified in all cores. Tsunami traces or effects are not directly mentioned. Changes in strata are opened to all possible events such as storm, tsunami, seismic tremor, and human triggered accidents. From this point, the study remains ambiguous for the sake of tsunami. However, in a part of the article, distortion of strata in a core was attributed to a seismic tremor or tsunami occurred in 5700-5600 BP.

Scheffers and Scheffers (2007) found traces of paleotsunamis along the coastlines of western Crete (Figure 2.1, WC-1). They include bimodal deposits containing large boulders associated with tilted biogenous notches and blocks up to 75 tons thrown onshore and embedded in strata of marine shells. They explored whether the source of these deposits belongs to 365 CE earthquake. They dated two more tsunami events at 5660- and 500-years BP using radiocarbon dating. They focused on littoral/foreshore deposits on-shore for about 150 km along the coastline, and they tried to differentiate these deposits from normal or storm waves. Dislocated large boulders contain lithophaga and vermetid borings. They think that large blocks cannot be transported without breaking and losing energy with the storm and they can not be transported from inland because these boulders have lithophaga and vermetid borings on themselves, which are littoral and foreshore organisms. Thus, it is interpreted that the only source can be a tsunami. They investigated five different locations in the western part of Crete and concluded the following evidence; chaotic shelly sands with floating boulders to dislocated huge plates of conglomerates, shell beds from a single event now buried under soil and dunes(5660 BP event), tilted notches in boulders, boulder ridges, dislocated beach-rock slabs, deposits of sands and (500 BP event) and higher and boulders dislocated for several 100 m and up to more than 25 m a.s.l. for tsunami imprints left on the shore. However, according to radiocarbon data, there is not any evidence pointing out 365 CE tsunami.

At Palaikastro in north-eastern Crete (Figure 2.1, EC), Bruins et al. (2008) report geoarchaeological tsunami deposits that are a mixture of geological materials, including volcanic Santorini ash, and debris of archaeological settlement. They

found various tsunami signatures in event deposits such as; 1) erosional contact with the underlying strata, 2) marine micro-fauna, 3) reworked building stone material in the lower part of the deposit, 4) imbrication of rounded beach pebbles, settlement debris, ceramic sherds and even bones, 5) multi-modal chaotic grain-size composition. In addition to geological and archaeological evidence, radiocarbon dating also indicates that the event deposits are coeval with the Minoan Santorini eruption and associated tsunami, i.e. ca. 1613 BCE. Field evidence at Palaikastro suggests that the waves due to Santorini tsunami were at least 9 m high.

Santorini Eruption in ca. 1613 BCE created approximately 26 m height tsunami waves and 200 m inundation towards inland along the coasts of Crete (Bruins et al., 2008; Dominey Howes et al., 2006; McCoy and Heiken, 2000; McCoy et al., 2000; Yokoyama, 1978). If it creates such big waves along the Crete coasts, it is likely to reach 1000 km away, Israel coasts (Goodman-Tchernov et al., 2009). Based on this motivation, Goodman-Tchernov et al. (2009) studied on the upper shelf off Caesarea Maritima, Israel, to find possible tsunami traces deposited after Santorini Eruption. They collected 4 different cores changing from 10 to 20 m water depth and analyzed in terms of particle-size distribution, planar bedding, shells of *taphoecoensis*, and dating (radiocarbon, optically stimulated luminescence and pottery). One of the cores consists of 40 cm thick sheet-like deposit. In the cores, they recognized min 1 max 3 events. While determining these events and differentiating tsunami deposits from storm ones, they used sorting and grain-size distribution among other tsunamigenic indicators which were previously used by other studies (Bruins et al., 2008; Dawson and Stewart, 2007; Dominey-Howes et al., 2006; Donato et al., 2008; Morton et al., 2007; Reinhardt et al., 2006) such as; erosional lower contacts, fining-upward particle-size distribution, imbrication of inclusions, individual or groups of molluscs, mixed wear and poor sorting of molluscs, change or distinctive microfossil assemblage (foraminifera), rip-up clasts, household goods and high-value anthropogenic cultural material displaced in marine context, rafted organics or pumice, unidirectional tilting of marine

installations, and well-rounded beach zone pebbles in deeper contexts. In this study, in 4 cores, they identified 3 tsunami layers with the one deposited after Santorini Eruption. In the cores, while storm layers are less visible, tsunami deposits can be clearly observed. Also, tsunamigenic deposits show poor sorting and a wider range of grain-sizes. Unique sorting of deposits in each core is also used as a tsunamigenic indicator in this study. Two of these events, except for Santorini, show different deposition content. These events have anthropogenic debris from the well-populated port city, but Santorini has not because when Santorini eruption occurred, Caesarea does not exist. Dating of these events was made by using ceramic finds, radiocarbon, and optically stimulated luminescence (OSL) dating. According to estimated ages, 1st event and 2nd event corresponds to 1.5 ka, 2 ka ago respectively, and the 3rd event is attributed to Santorini tsunami, which is approximately in 1613 BCE.

Alpar et al. (2012) considered that low-lying coastal areas of Dalaman delta beach as a target site to investigate sedimentary traces of past tsunamis triggered especially by the earthquakes on the Pliny and Strabo trenches (Figure 2.1, D). Their study is based on marine-sourced biomarkers such as phytoplankton, zooplankton, dinoflagellates, and bacteria to find tsunami traces. In their study, they have taken samples from sidewalls of the trench to identify major lipid biomarkers such as fatty acids and sterols. Elemental analyses of normal and branched alkane, fatty acid, sterol biomarkers, and other diagnostic indicators were made. For instance, while long-chain $> C_{24}$ fatty acid biomarkers are used to identify terrigenous plant provenance (Colombo et al., 1997; Parrish et al., 2000), polyunsaturated fatty acids (PUFAs) with 16, 18, 20 and 22 carbon atoms are frequently used as planktonic organism biomarkers (Stefens et al., 2007). Additionally, quantitative estimation of biomarkers and deterministic ratios (abundance of S-containing compounds vs pristine (Pr): phytane (Ph) ratio) were used as evidence to show up tsunamigenic impacts. The relative abundance of S compound can be used to determine the provenance of the species either is the freshwater or marine origin (e.g. pristane/phytane ratio against the S-containing

parameter). They opened a trench just near the previous studies and taken samples from 5-15 cm-thick sandy units and above and below of it. Although there was no fossil content in these units, there may be fingerprints of biomarkers. Thus, they looked into sediments' chemical and biogenic content. In the end, they reached a powerful data showing marine fingerprints as a result of biogeochemical analyses in the middle of the section, which gives date 1481 CE.

Similar to Alpar et al. (2012), Papadopoulos et al. (2012) conducted a study in Dalaman to find geological evidence of tsunamis. The study area is located at the undisturbed coastal wetland and protected from the sea with a sand barrier. In this area, they opened a trench 240 m from the shoreline and identified 3 sediment layers, located at 0.30, 0.55 and 0.90 cm depth. In general, these layers are composed of silty mud and contain terrigenous mollusc fossils of genus *Helicostyla*, *Sucinea*, *Pormatias* and *Pseudotaches*. All these layers show landward thinning and erosive contact with the underlying non-marine layer. Radiocarbon dating could only be applied to the 2nd sand layer since carbonaceous material only exists in that layer. A wood fragment located upper part of the 2nd layer was dated. Estimations show CE 1473±46 which fits well with the historically documented large earthquake and tsunami event of CE 1481. Since, in other layers, there was no other material for dating, the extrapolation method is used while making interpretations for their ages. The sedimentation rate is accepted as 0.13 mm/yr. After estimations, “sand layer 3” could be attributed to 1741, and “sand layer 1” to 1303 big tsunami events. They also mention the strong tsunami of 1609 was missing from the Dalaman stratigraphy. Possible reasons are; i) the 1609 tsunami failed to inundate the Dalaman coastal zone studied, ii) the tsunami inundated this zone but did not leave behind tsunami deposits in the trenching site, and iii) the tsunami inundated and deposited sediment at the trenching site but the sand layers were eroded.

Öğretmen et al. (2015) conducted a study in Silifke, south Turkey (Figure 2.1, Si). Boulders about 1.3-3 tons lying along the coast are used as geomorphological evidence for a high-energy wave event in Yeşilovacık region. Turkish coastal areas

are not prone to produce storms which are capable of carrying such blocks. Even if it happens, the area where boulders exist is in semi-protected embayments, which is capable of attenuating the energy of storm waves. Thus, they pointed out another possible disaster, i.e. tsunami. The block 2.6 m a.s.l was encrusted with vermetids which shows a provenance from an intertidal marine environment. Since these boulders have step-like morphology, Ögretmen et al. think that their transportation mechanism must be consistent with saltation instead of rolling or sliding. Additionally, several examples also exist in Narlıkuyu region. One of them lies on the marly limestones 0.8 m a.s.l and 6 m inland with lithophaga borings. It is about 1 m in diameter and weighs around 1.3 tons. Lithophaga borings also show its provenance as an intertidal environment. The data obtained from AMS C14 dating on vermetids shows that the emplacement of the blocks should be later than CE 1950. It reminds 10 September 1953 Paphos earthquake occurred along the SW Cyprus subduction zone, and Paphos transform fault. This earthquake has $M=6.2$, which has not enough energy to produce such waves. Thus, they think that the probable reason for these boulders to have been transported can be a local landslide-generated tsunami seismically triggered by Ecemiş Fault. In this manner, they think that in order to resolve this issue, high-resolution bathymetry maps for Cilicia trough bathymetry the Anatolian margin of the Cilicia trough to accurately model the near-shore amplification of tsunami waves can be helpful.

Shah-Hosseini et al. (2016) made a study along the Mediterranean coast of Egypt between Alexandria and Marsa-Matrouh at four distinct sites (Figure 2.1, Ma). Different from the others, they do not state on only tsunami waves, but also, they try to find out large wave impacts on transportation of medium to large boulders weighing up to 23 tons toward 40 m inland. According to radiocarbon dating, only one site could give an anticipated result for tsunamis, CE 1303. The other 3 sites give younger ages. In a hydrodynamic model applied by Iskander (2013), in order to transport these boulders, while tsunami waves need to be min 2.6 m in height, storm waves need to be min 10 m. Since 1303, there has not been a tsunami strong enough to carry these boulders in this region. Accordingly, with the hydrodynamic

model, storms were capable of carrying these boulders in the Mediterranean during the Little Ice Age between the sixteenth and nineteenth centuries CE (e.g. Dezileau et al. 2011; Sabatier et al. 2012; Shah-Hosseini et al. 2013; Dezileau and Castaings 2014). Thus, the boulders existing on the other 3 sites are thought to belong to multiple intense storms recurred in every 100 years, which are estimated by the wave height model by Iskander (2013).

Ashkelon in Israel (Figure 2.1, As) has existed since ancient times and contains many natural and anthropological deposits (Hoffmann et al., 2018). Since those times, historical sources have recorded many important events, including paleotsunami events. Hoffman et al. (2018) conducted a study at the base of an eroding coastal archaeological section and realized a sedimentary sequence showing waterborne transportation. The sedimentary sequence in the section consists of fining-upward sequences, rip-up clasts, imbricated inclusions, fine mud layers, microfauna (foraminifera) showing marine-origin deposits, and broken diagnostic pottery from the 4–5th century BCE. They correlated these deposits with river and storm deposits. Then, about 100 m inland, at 2.0-2.4 m a.s.l., they looked in the sampled profile and have not seen any river features in itself. Additionally, according to modern observations, today's' storms are effective in < 75 m inland and leave its deposits maximum about this distance. Contrary to claim about the deposits belonging to catastrophic event proposed by Rosen (2008), based on the results, they interpreted these deposits as unrecorded tsunami occurred in 4-5th century BCE.

Tyuleneva et al. (2018) also studied on the sediment cores collected offshore at Caesarea, Israel (Figure 2.1, Ca) in order to find backwash deposits of tsunamis, and they chronologically improved the results of Goodman-Tchernov et al. (2009). Granulometry, mineralogical studies, x-ray diffraction (XRD), x-ray fluorescence (XRF) and Fourier transform infrared spectroscopy (FT-IR) were performed to reveal and characterize tsunami deposits. The sediments were also dated by the radiocarbon method. Tsunami related deposits are found to be poorly sorted, rich in

bivalve shells, and Zr, Ti and Fe. They conclude that they found sedimentary traces of tsunamis in CE 746, 115, and 1613 BCE (Santorini).

Salama et al. (2018) studied two different lagoons at Kefr Saber and El Alamein village (Figure 2.1, KS and EA). They searched sedimentary records of tsunamis in these sites. They obtained the data from the field by using geomorphological imprints and opening trenches along the coastal area. They opened 5 trenches (2x1 m, and 1,5 m depth) at Kefr Saber and took 12 cores (1 to 2.6 m-long) from the El Alamein site. These studies are carried on summer when lagoons are dry. Carried studies on the field are the log of sedimentary sections using X-rays, grain size and sorting, total organic and inorganic matter, bulk mineralogy, magnetic susceptibility, and radiocarbon dating for 46 samples to identify past tsunamis records. Based on the results, they report 4 tsunamis; CE 365, 1303, and 1870 earthquake. The 4th tsunami event (1126-1434 BCE) that they found their traces in the cores is not reported in tsunami catalogues. In these sites, tsunami layers are characterized by fine and coarse sand mixed with bioclasts. They have seen the white sandy layer with broken shells as coarse-grained in fining trend towards inland in all trenches and cores (except 5th core), although the sites are ~200 km apart from each other. First event layer is 7.5 cm-thick and poorly sorted white sandy deposits with broken gastropods and lamellibranch (shell) fossils which show the bi-modal grain-size distribution and low-magnetic susceptibility. 2nd event layer is about 13 cm-thick and consists of white sandy deposits intercalated with laminated coarse brown sand, which also show very poor sorting of sediments and low magnetic susceptibility. 3rd layer is 25 cm-thick composed of grey sandy clay, with a high peak of magnetic susceptibility. All these layers were rich in organic content and composed of poorly sorted sediment. Low magnetic susceptibility values point out tsunami layer because such deposits consist of more carbonates and quartz than the underlying layer so gives low magnetic susceptibility values.

Werner et al. (2018) conducted multi-proxy studies to find tsunami imprints left behind on the Sougia and Palaiochora coastal plains in Crete (Figure 2.1, WC-2).

They pursued sedimentological, geochemical, geochronological and microfaunal methods in this study. To the study, they started with geophysical investigations to understand stratigraphical structures and to discover bedrock topography. Then, they obtained stratigraphy by taking ten vibrocores from the field, and they are correlated with geophysical data. They applied grain-size distribution analyses and looked into microfaunal assemblages to differentiate autochthonous units from allochthonous ones. By using radiocarbon dating, they had a chance to get the expected date and make a chronological order. They presented essential clues showing extremely high-energy wave impacts in units, which are basal erosional contacts, fining upward trends in grain-size, impulse-controlled multiple-layer sequences, peaks in the Ca/Fe ratio, and evidence of allochthonous marine microfauna. At the Sougia, they took five vibrocores from the coastal plain and identified four different units amongst all cores. One of them represents the tsunami deposition level. Tsunami deposits which were recorded in all cores have erosional contact with underlying units and consist of fining-upward sediments. According to geochemical analyses applied on selected one core, they observed that the Ca/Fe ratio made a peak in tsunami deposits, and magnetic susceptibility is slightly decreased as well; both are implying marine-origin sediment intercalation. Foraminifera species, at this level, is highly abundant but underlying units do not have any. Additionally, underlying units have voids of microfossils, which refer to the abrupt deposition of marine sediments. At the Palaiochora, they studied on 4 vibrocores and identified 5 different units. Two of them were taken from the present beach; the others were taken from top of the promontory, which was 4.25 m under water before 365 CE earthquake after which it uplifted about 7.75 m. Researchers detected two event layers in cores in Palaiochora. While the cores taken from beach contain two events, in the promontory cores, only one event is recorded. One event is common in all cores. For the first event seen in all cores, tsunami unit overlying erosional contact is characterized by two fining-upward sequence consisting of coarse to fine sands. Microfaunal fossil fingerprints in this sequence show that these deposits are allochthonous and marine origin. According

to geochemical analyses applied on selected cores (1 core from beach, the other one from promontory), Ca/Fe ratio peaked at tsunami level. This level shows two fining-upward sequences implying 2 wave-pulses in beach cores but 1 wave pulse in promontory cores. They explain this situation as that the other high energy deposits may have been eroded and/or reworked in time. Indeed, they think that in order to explain exact reason, this area needs more detailed geological investigation. 2nd event deposits in Palaiochora cores, which are only seen in beach cores, are composed of poorly sorted sediments showing bimodal grain-size distribution, which was regarded as a typical of high-energy tsunami-type inundation (Scheffers and Kelletat, 2004; Scheffers and Scheffers, 2007), however, they interpreted 2nd event deposits as a latter phase of extreme-high-energy event deposits related with turbulent flow conditions. According to radiocarbon and OSL dating, 1st event level is directly pointing out CE 365 tsunami.

Avşar (2019a) performed a study concerning the sedimentary records of paleotsunamis in Ölüdeniz Lagoon, which is one of the most suitable depositional environments to preserve tsunami records, located in Fethiye, in Turkey (Figure 2.1, Ö). He presumes that if a tsunami wave comes towards this lagoon, sand spit should be overwashed by the tsunami wave and sediments carried as suspended load with water should be deposited in the lagoon. So, the terrigenous content should be higher in the tsunami deposits. He took three short gravity cores of 84 cm, 99 cm and 102 cm in length. Along the cores, which are mainly composed of yellowish-brown sandy-silt, he realized 3-5 cm-thick reddish-brown intercalations that were revealed by dividing red values to blue and green values along the core RGB images. ITRAX micro-XRF scanning along the cores also revealed that the intercalations are rich in elements representing terrigenous minerogenic clastics (e.g. K, Ti, and Fe) compared to the one representing biogenic/chemical carbonates (e.g. Ca and Sr). This observation implies that the intercalations are related to the sudden influx of terrigenous sediments into the lagoon. The chronology of the cores was obtained by using ¹³⁷Cs and ²¹⁰Pb dating and stratigraphical correlation. Accordingly, he concludes that the three distinct intercalations in the cores

temporally correlate with historically well-known tsunamis in CE 1741, 1609 and 1303.

CHAPTER 3

RESULTS

3.1 Visual Inspection of the Cores

In the beginning, before element-based XRF analysis, all cores were inspected visually along the core images. An abrupt change in color, grain-size, or density of the sediments within the cores can be used as visual proxies for better understanding of the geological imprints left from the past. In this investigation, firstly, radiographic and optical images obtained by ITRAX-micro XRF scanning were examined along the cores to detect the sedimentological traces of past tsunamis.

There is a dominance of greenish-yellowish colors in all of the cores (Figure 3.1-3.4). Background sedimentation mostly consists of silty and clayey units. In some levels, intercalation of reddish-brownish layers is also observed along the cores. Careful analysis of the reddish layers revealed that they contain small amount of charcoal. The presence of these intercalations within the background sedimentation implies that some extra-basinal materials were transported from somewhere else and deposited within the sequence. At some levels of the cores, these layers are visible to the naked eye and they have the potential to be event layers in the sequence.

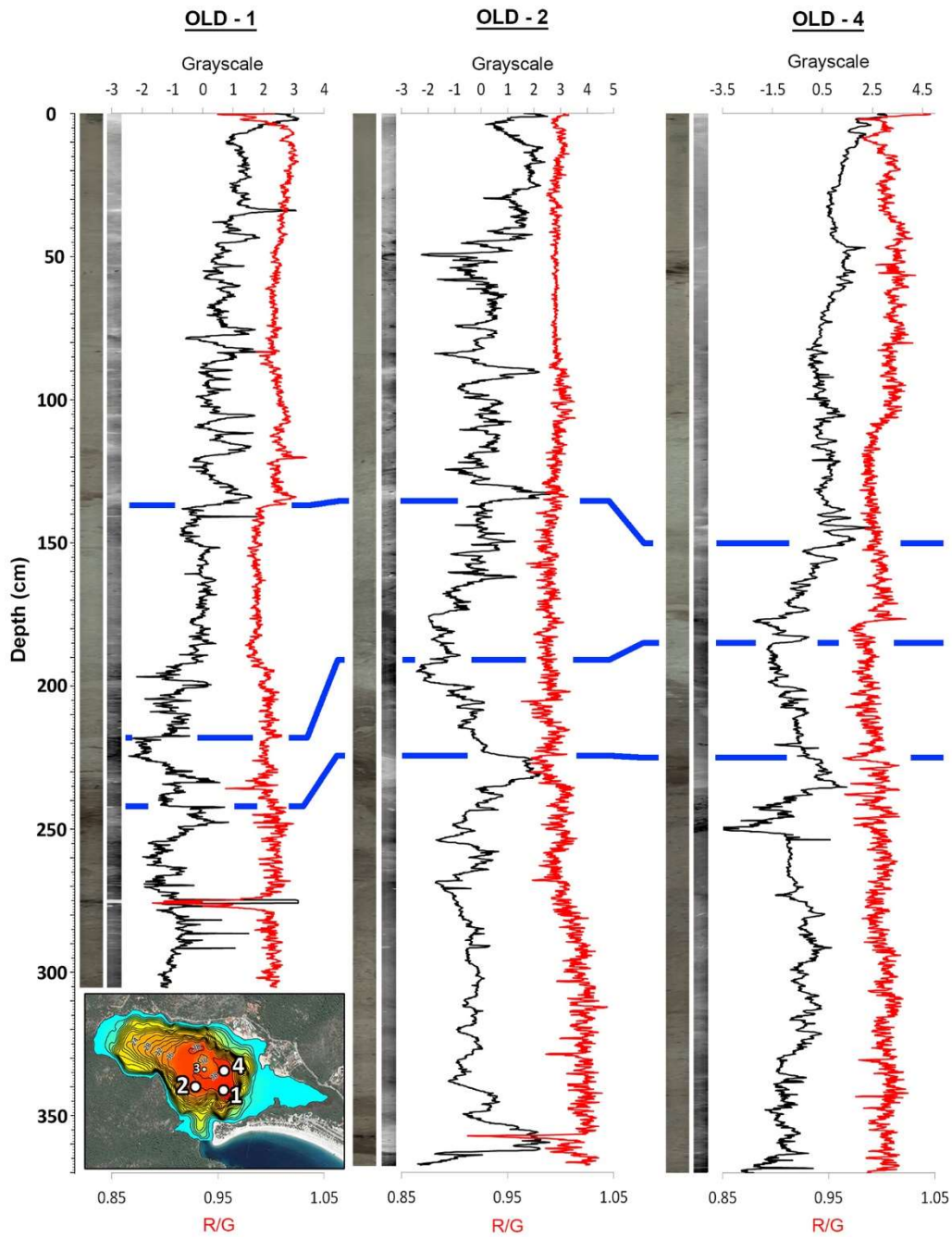


Figure 3.1. Optical and radiographic images of the cores OLD-1, OLD-2 and OLD-4. Grayscale profiles of along radiographic images and Red/Green ratio profiles along RGB images are also presented. Blue lines illustrate levels that can be correlated even based on core images. Widths of images are three times exaggerated in order to ease visual inspection.

Close-up views of optical images for each core are represented in the following Figures 3.2, 3.3 and 3.4. Background sedimentation is in yellowish-grey color. Intercalation of background sedimentation and carbonaceous materials are apparently seen in reddish-brown color.



Figure 3.2. Close-up view for OLD-1 optical image.



Figure 3.3. Close-up view for OLD-2 optical image.



Figure 3.4. Close-up view for OLD-4 optical image.

In order to evaluate the event levels more precisely, R and G values of the levels were used to estimate the redness of the core. Red and Green pixel values of the optical images were extracted by using MATLAB software and in order to determine redness of the core, red values are divided into green ones to correlate those with potential event layers. Aftermath, it is obviously seen in R/G curves, which shows proportional increase at reddish-brownish layer levels, by giving anomalies in the positive direction. Besides, disorderly distributed charcoals (dark patterns in the core) within reddish-brownish layers imply terrigenous organic matter input. During the transportation, these charcoals were accompanied by allochthonous units. Radiographic images show density of deposition units. While darker layers indicate dense materials, lighter layers indicate relatively less dense materials. As it is in the Figure 3.1, as the layers' color turn into reddish-brown, corresponding layer becomes lighter. Considering that the density of organic matter is lower than deposited units, then, it strongly implies organic material input to the lagoon. Grey scale values also support this hypothesis. The lighter colors, the higher RGB values in grey scale bar. Thus, light color in radiographic images correspond positive anomalies in grey scale curve. Considering all entire clues, it is indicated that allochthonous units along the core have terrigenous origin.

By using all clues obtained from optical and radiographic images, three different sedimentological imprints are visually seen in each core. In OLD – 1, these imprints are observed at 130-135 cm, 220-225 cm and 240-255 cm depth, in OLD – 2 at 130-137 cm, 190-195 cm and 225-240 cm depth, and in OLD – 4 at 145-152 cm, 180-185 cm and 227-242 cm depth. Every three levels can be correlated with each core and give the same sedimentological event. Depending on the sedimentation rate, their levels show a difference. Each event is identified, correlated and schemed in Figure 3.1. However, we only can correlate the middle sections of the cores. The upper and lower layers seem ambiguous and do not contain sufficient data to make a correlation. Thus, we need to extend our study one more step. At this stage, XRF is getting importance. By using XRF data,

elemental ratios profiles of the cores are used to support and improve the stratigraphical correlation between the cores.

3.2 Micro-XRF Data

Following the visual inspection, XRF analysis is made on the cores. Profiles of elements K, Ti, Fe, Zn, Rb, Si, Ni, Mn, Cr, Ca, Cl, S, Br and Sr were determined by ITRAX, and curves for these elements are presented in Figure 3.5. Due to machine limitations, some elements could not have been estimated such as Al, Na and Ba. This method is basically applied in this study to investigate terrigenous matter input into the lagoon and make this investigation precisely. Thus, the efforts in this study are mainly concentrated on K, Ti, Fe and Zn elements representing terrigenous minerogenic clastics and Ca representing basically biochemical carbonates precipitated from the water column.

It is expected that there must be an increase in terrigenous materials, but a decrease in biochemical materials precipitated from the water column. During such extreme wave events, the hypothesis is that terrigenous materials are deposited abruptly so biochemical materials or dissolved rock materials floating in the water do not have time to precipitate. In the light of these clues, two potential events in OLD – 1, at 130-135 cm and 235-255 cm depth, three potential events in OLD – 2, at 205-240 cm, 255-265 cm and 345-365 cm depth, four potential events in OLD – 4, at 48-60 cm, 100-106 cm, 205-245 cm and 305-325 cm are detected (Figure 3.2). All events show a sudden increase in K, Ti, Fe, Zn, Rb, Si, Ni, Mn, Cr curves, and a sudden decrease in Ca values. Since Cl, S, Br and Sr do not give good results, their results are excluded from the study. All these peaks enable us to correlate with the grey-scale curve, R/G curve, optical and radiographic images, but it will be discussed in the discussion part.

Despite being located nearby each other, there is a difference in the recorded number of events in each core. This may be related to the intensity of the events.

Following getting radiocarbon data and matching up with potential events (determining ages), interpretation will be easier.

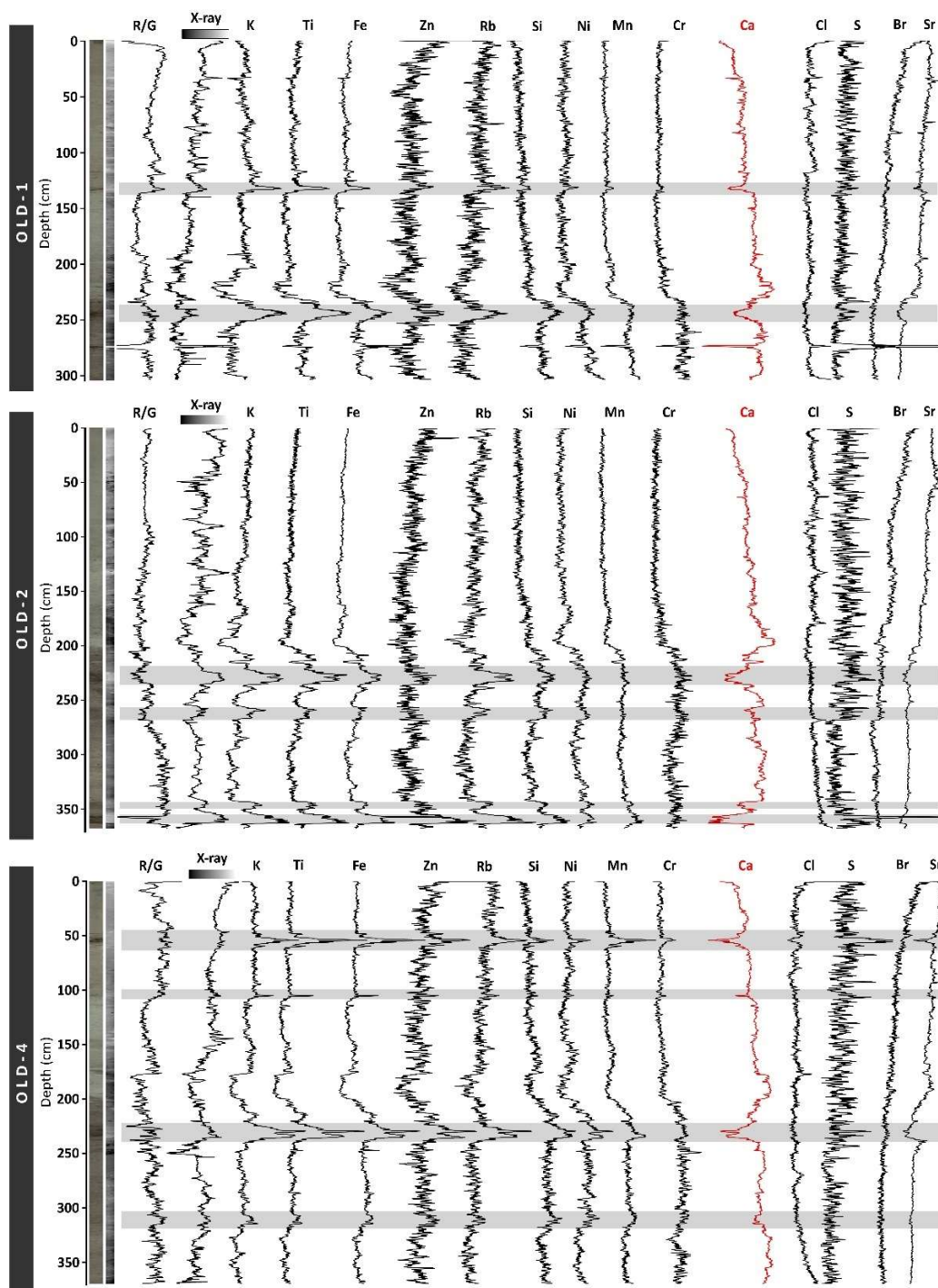


Figure 3.5. XRF data for each element obtained from OLD -1, OLD -2 and OLD-4. R/G and X-ray grayscale curves are also provided.

3.3 Radiocarbon Data

In the scope of the study, dating event layers has great importance to firstly check the temporal correlation between the historical tsunami records and the detected sedimentary events, and secondly to determine the dates of pre-historical events so that we can better evaluate the existence of regular recurrence of tsunamis in the Eastern Mediterranean. Radiocarbon dating is very suitable for this study because terrigenous plant remains were found in the cores. There were 3 in OLD-1, 2 in OLD-4, and 1 in OLD – 2.

After halving the cores, they were visible with the naked eye, and for radiocarbon dating, they were picked from the cores. This plant remains, which are Pinus branch pieces, are very valuable in terms of getting reliable dating results free of hard water effect. Long reworking time in the catchment before the deposition can also be ruled out because a significant part of the area surrounding Ölüdeniz Lagoon has steep slopes covered with Pine trees. Thus, a wood piece dropped from a tree would quickly be transported into the lagoon and deposited, which minimizes reworking effect. Information on radiocarbon dating on these samples is presented in Table 3.1.

The terrigenous origin of the dated plants remains is also confirmed by their $\delta^{13}\text{C}$ values. According to Stuiver and Polach (1977), while aquatic plants have $\delta^{13}\text{C}$ values around -15 ± 5 , terrigenous plants have values around -26 ± 4 . As it is seen in Table 3.1, $\delta^{13}\text{C}$ values of dated samples are in between 28 ± 4 . Hence, they are terrigenous. In Table 3.1, results of 6 radiocarbon dating, calibrated results, and $\delta^{13}\text{C}$ values are presented.

Collecting multiple cores from the lagoon also increased the chance of finding terrigenous organic matter. However, each core is from different stratigraphical levels of the Ölüdeniz sequence and belongs to different ages. For this reason, the inter-core stratigraphical correlation should be done accurately.

Table 3.1 Information on the radiocarbon samples and dating results.

Lab ID	Sample ID	Depth in Core (cm)	$\delta^{13}\text{C}$	Radiocarbon Age (BP)	Calibrated Date (BC/AD)	
R1	Poz-102135	OLD-1-1 37	37	-24.7	45 ± 30	1806 ± 113 AD
R2	Poz-97889	OLD-1-4 26	230.2	-26.9	1555 ± 30	496 ± 75 AD
R3	Poz#2-97784	OLD-4-4 2	273.1	-29	1740 ± 30	311 ± 75 AD
R4	Poz-97890	OLD-1-4 72	276.2	-27.7	1895 ± 30	134 ± 82 AD
R5	Poz#2-97785	OLD-4-4 76	347.1	-30.3	2000 ± 30	8 ± 63 AD
R6	Poz#2-102152	OLD-2-4 97	355.3	-31.2	2030 ± 30	52 ± 105 BC

Since the amount of C^{14} in the atmosphere changes through time, radiocarbon measurement results from the laboratory need to be calibrated. After getting the results, obtained values were calibrated by using Oxcal program. Intcal13 version of the calibration curve was used in this study. In Figure 3.6, calibration results for each sample are shown. In each graph, red polygons along y-axes represent the normal distribution of results from the radiocarbon laboratory with errors, and grey polygons along x-axes are the projection of red distributions by calibration curve (blue lines).

In graph R1, organic matter is picked from the core OLD-1, at 37 cm. Its calibration gives two probabilities, 21% and 74.4%. In order not to miss any data, two probabilities are considered, and the calibrated date of the sample was determined to be 1806±113 CE. In graph R2, the plant was found in the core OLD-1, at 230.2 cm depth. After the calibration, the result is 496±75 CE with 95.4% probability. In graph R3, the calibrated result is 311±75 CE with 95.4% confidence, for the plant from OLD-4 at 273.1 cm. In graph R4, the calibrated result is 134±82 CE for the plant in the core OLD-1 at 276.2 cm with 95.4% probability. In graph R5, we also got two probabilities for this result. Since the second probability value is very low, 0.8%, it is ignored. Thus, our calibration result is 8±63 CE for the plant in the core OLD-4 at 347.1 cm with 94.6% probability. In graph R6, calibration is applied on the single plant remain existing in the core OLD-2 at 355.3 cm. As it is in the graph R6, we obtained two probabilities, %2.7 and %92.7. Both probabilities were taken into consideration

that is why the error in these calibrated dates is a little bit higher in terms of other results. The calibration result for sample R6 is 52 ± 105 BCE.

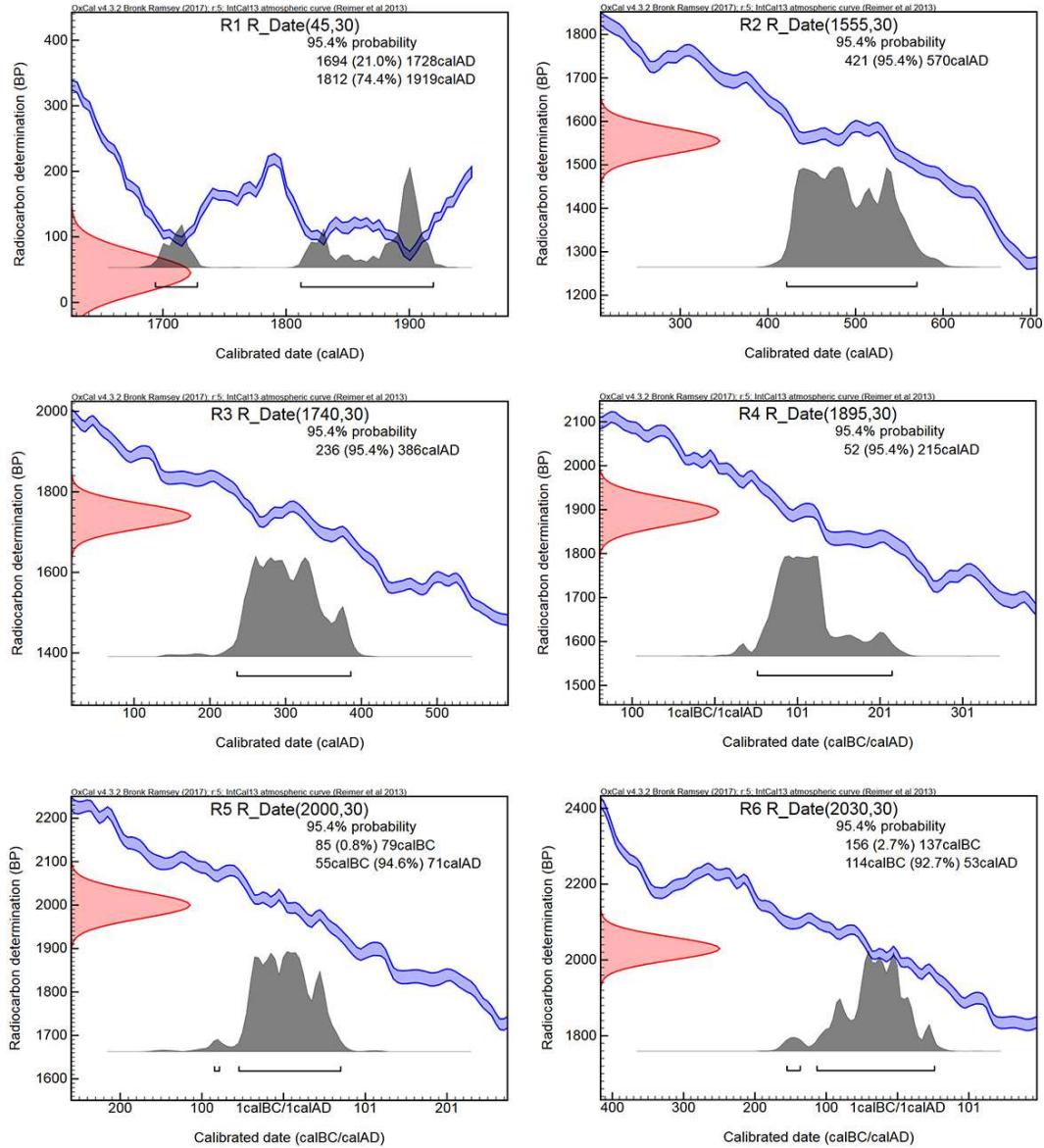


Figure 3.6. Radiocarbon calibration results from Oxcal software with Intcal13 calibration curve.

CHAPTER 4

DISCUSSION

In order to claim that the sedimentary events and paleoenvironmental record revealed from Ölüdeniz Lagoon is meaningful and reliable, the cores should be carefully correlated. So that, we can say that geochemical information revealed is basin-wide, and events are not because of local mechanisms like sediment focusing or coring deformations. For this reason, the cores were both visually and geochemically inspected in detail in order to achieve a reliable stratigraphical correlation, and to detect possible sedimentary events intercalated with the background sedimentation.

Although visual correlation is limited, geochemical data (i.e., ITRAX data) is highly useful to correlate the cores. Basically, Ti/Ca ratio profiles, which clearly expose sedimentary events, were used for stratigraphical correlation (Figure 4.1a). The cores could be connected to each other by 12 stratigraphic levels; grey lines in Figure 4.1a. It is clearly seen that the longest sequence is recovered by OLD-2. Accordingly, the depth scales of OLD-1 and OLD-4 were adjusted in order to stratigraphically match them with OLD-2, and to be able to present them in an overlapped way so that success of correlation can be checked easier. R/G, X-ray grayscale and ratio profiles of K/Ca, Ti/Ca, Fe/Ca and Zn/Ca are overlapped for three cores and presented in Figure 4.1b. It is obvious that the correlation is successful.

As a result of getting correlated results, 8 possible sedimentary events are observed (Figure 4.1b). In each elemental ratio, anomalies are apparently seen. However, events are recorded depending on the core locations in the lagoon. For example, the youngest two events seen in OLD-4 are not clearly seen in OLD-2. However, OLD-2 consists of the last two events not recorded by any core because of its

longer stratigraphic age. At some places, elemental ratios are matching up with R/G curve and grey scale curve.

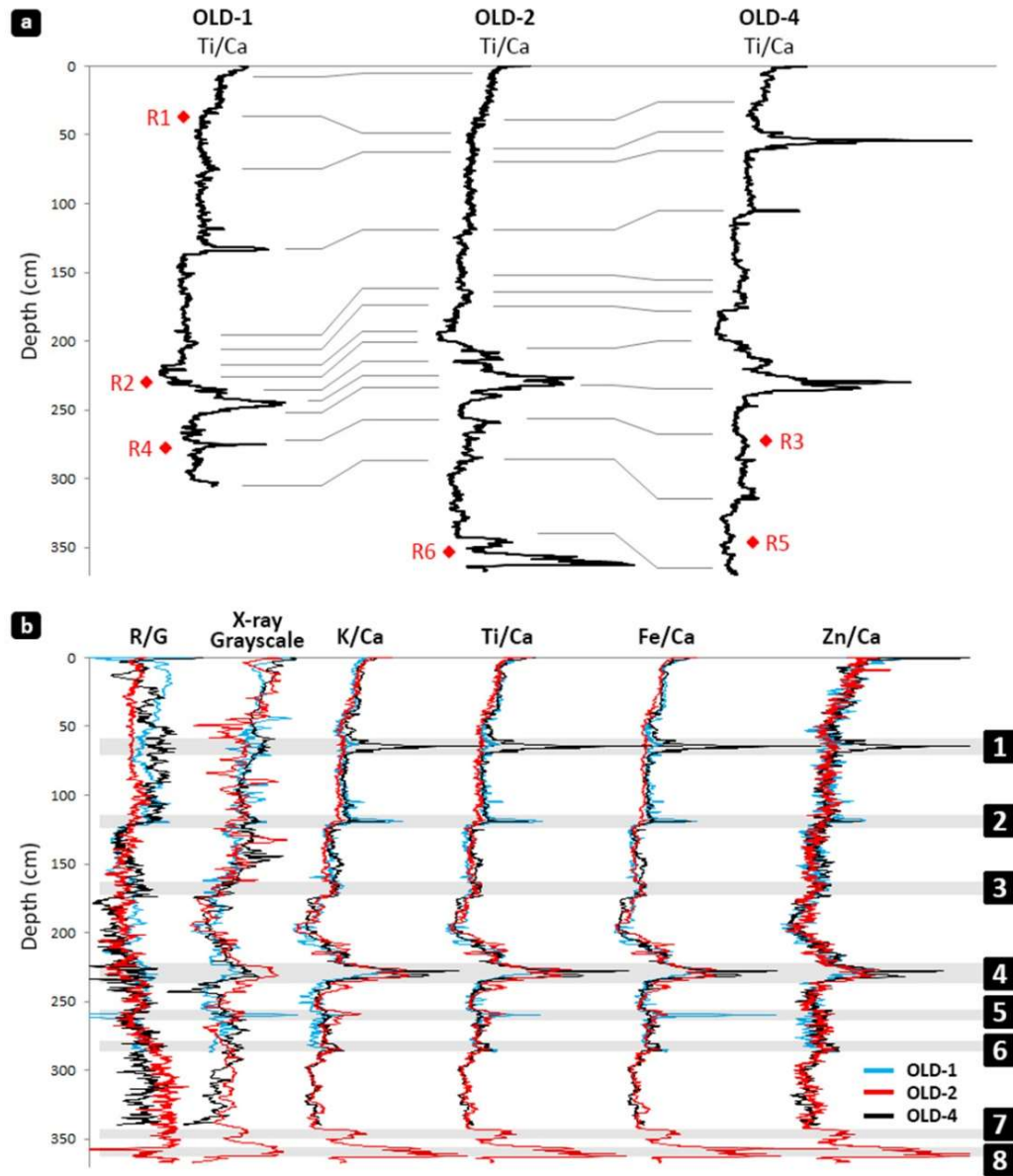


Figure 4.1. a) Correlation of three cores by means of Ti/Ca profiles. Locations of radiocarbon dates (R1 to R6) are also shown. Note that the longest sequence is covered by OLD-2. b) Different proxies of three cores overlapped after modifying depth scales of OLD-1 and OLD-4 with respect to OLD-2. The success of stratigraphical correlation is obvious. Presence of eight sedimentary events (Grey bars 1 to 8) can be proposed.

Especially, the grey-scale curve creates beautiful geometry fitting with elemental ratios. According to Figure 4.1, we see that 5 events in OLD-1, 5 events in OLD-2, and 6 events were recorded in OLD-4. 4th, 5th and 6th events are recorded by all cores in common. Of which, 4th event is evident in all cores.

As the stratigraphical correlation is successfully reached, the next step is to construct the sediment chronology. The top 140 cm of the sequence of this study gives very similar results with Avşar (2019a) (Figure 4.2). When we correlate our study with an independent one (Avşar, 2019a), we see that these directly point out historical tsunamis, occurred in 1741, 1609 and 1303, which are shown as E1, E2 and E3 in Avşar (2019a). Accordingly, it can be claimed that 42 cm, 63 cm and 119 cm depths of this study corresponds to CE 1741, 1609 and 1303, respectively. In addition to radiocarbon dates, this information is used while constructing the age-depth curve presented in Figure 4.3. Despite being very close to Avşar (2019a) coring locations (Fig. 1.9c), in our study, 1741 CE tsunami is not recorded in none of the cores of this study. Contrarily, CE 1609 and 1303 tsunami anomalies are seen better than Avşar (2019a) records (Fig. 4.2).

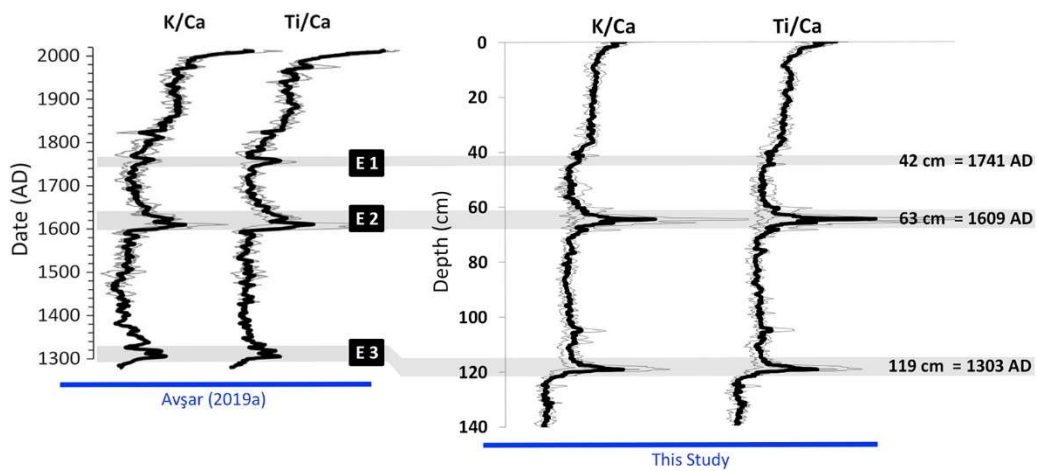


Figure 4.2. Correlation of K/Ca and Ti/Ca profiles of Avşar (2019a) with the profiles of this study.

After having all results, we designed an age-depth model showing calibrated radiocarbon ages with error bars, and the average of Ti/Ca profile for all cores.

When we put Avşar (2019a) data on the figure, it is observed that our anomalies are matching up with Avşar dates, which directly shows us the sedimentary event levels and dates. Avşar (2019a) supports our hypothesis, i.e., each significant anomaly in Ti/Ca represent a sedimentary event. Based on this information, our age-depth model is constructed. When sedimentation rate (SR) of 0.11-0.14 cm/yr was assigned down to ca. 225 cm, and SR of 0.18-0.20 cm/yr for the rest of the core, the age-depth curve reasonably passes all radiocarbon dates and correlation points with Avşar (2019a) (Figure 4.3).

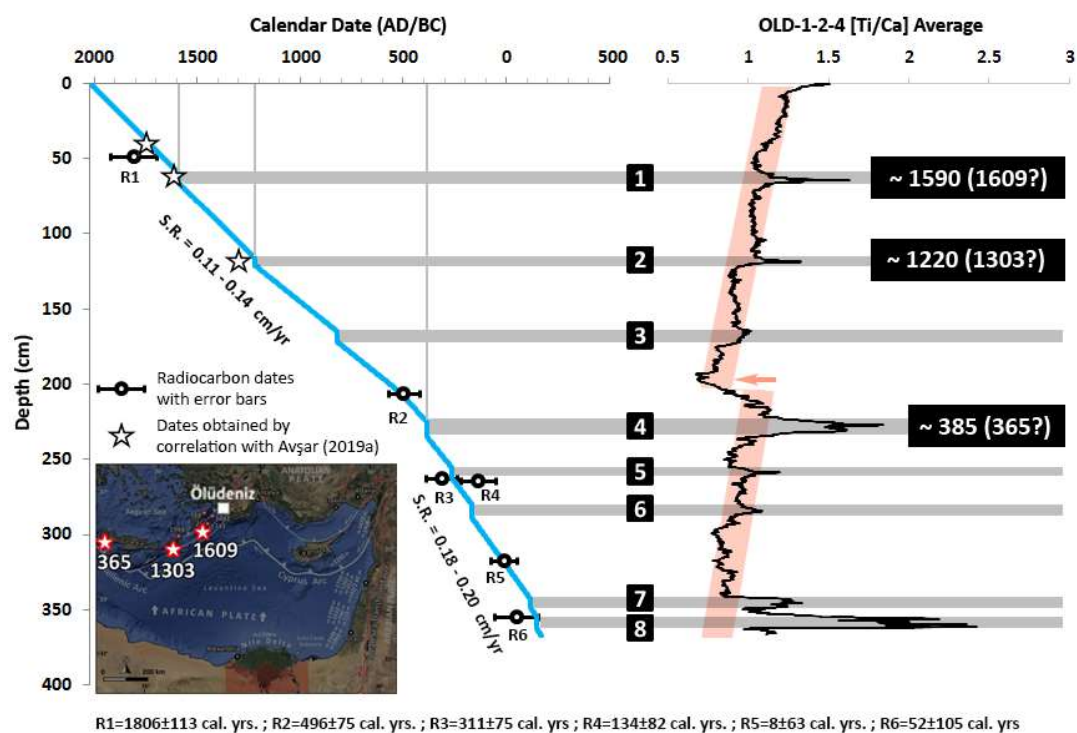


Figure 4.3. Age-depth curve constructed based on radiocarbon dates and correlation with the record of Avşar (2019a). At depths corresponding to the anomalies along Ti/Ca profile, the age-depth curve is vertical, meaning that these anomalies are assumed to be sudden depositional events.

An important assumption while constructing the age-depth curve in Figure 4.3 is that the anomalies seen along the Ti/Ca ratio profile are sudden depositional events so that those levels appear vertical on the age-depth curve. Another assumption was

about the change in sedimentation rate at around 205 cm, which is seen as a shift in Ti/Ca ratio profile towards lower values. This shift implies that lower amounts of Ti and hence lower amounts of terrigenous clastics entered into the lagoon, which means lower sedimentation rates can be expected since the shift. This is consistent with the sedimentation rate assumptions.

According to the age-depth curve presented in Figure 4.3, three youngest and most significant anomalies along the Ti/Ca profile (i.e., 1, 2, 4) seem to temporally correlate with well-known historical tsunamis in CE 1609, 1303 and 365. This observation implies that tsunamis may result in a sudden terrigenous clastic influx into the lagoon or sudden decrease in carbonate deposition in the lagoon, as previously suggested by Avşar (2019a). This hypothesis can be schematized like in Figure 4.4.

As it is seen Figure 4.4a, before the tsunami, in stagnant water conditions, terrigenous clastics transported from the catchment by surface runoff, and biogenic/chemical carbonates (Ca) from the water column are deposited together. During the tsunami (Figure 4.4b), when the waves overwash the sand spit and inundate to the lagoon, terrigenous clastics abraded from near shore and sand spit are transported into the lagoon-like a sediment cloud in the water. Coarser clastics cannot be transported for long distances, and they deposit just behind the sand spit. However, the finer part can be dispersed all over the lagoon. Immediately after the tsunami (Figure 4.4c), once the turbulence of the water ceases, this fine-grained sediment cloud is quickly deposited. In the meanwhile, since the deposition is very fast, there is no time for the water column to contribute the sedimentation in terms of biogenic or chemical carbonates. This mechanism would surely result in significant anomalies in Ti/Ca values.

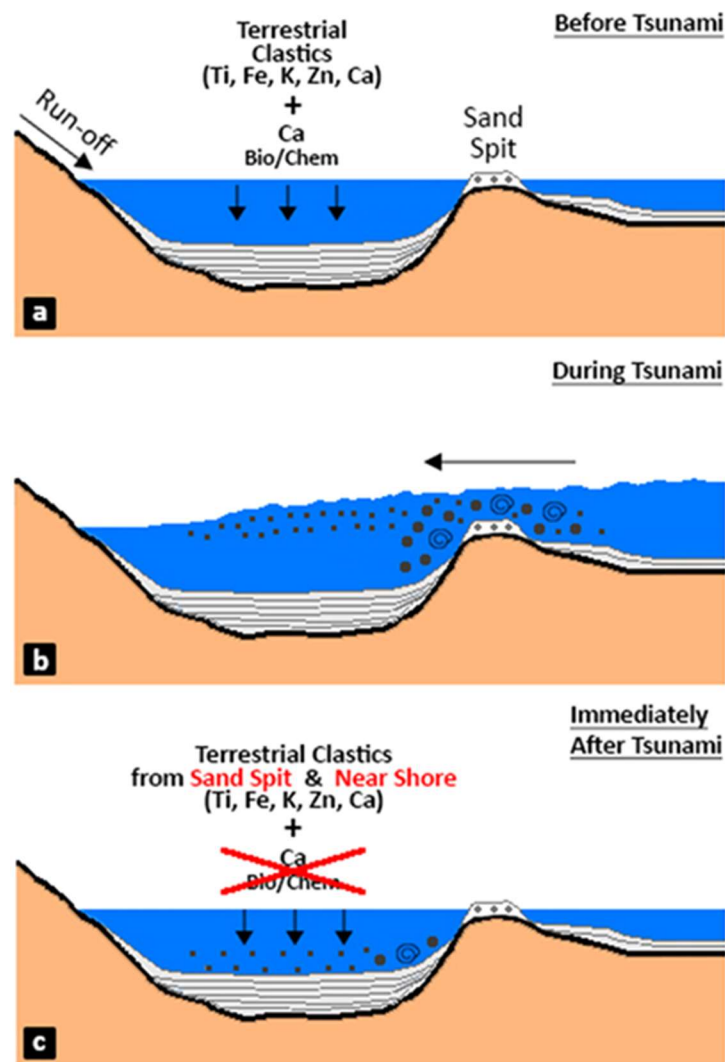


Figure 4.4. A mechanism explaining the possible relation between tsunamis and Ti/Ca anomalies in Ölüdeniz sedimentary sequence.

There are other natural events that could result in Ti/Ca anomalies. For example, an earthquake-triggered mass-wasting event on the slopes of Ölüdeniz Lagoon may produce a seismo-turbidite that can travel to the middle parts of the lagoon and deposit extensive clastic material. Since this kind of deposition would be very fast, there would be no time for biogenic/chemical carbonates to deposit from the water column, which would result in Ti/Ca anomalies within the background sediments. However, as it is presented in Figure 1.8a, there is no well-defined active fault around Ölüdeniz Lagoon. The highest PGA created during the last 120 years was

around 50 cm/s^2 because of an $M=6$ earthquake in 2012. Although this PGA level can be assumed to have potential to trigger subaqueous mass wasting events (e.g. Avşar et al., 2016), there is no Ti/Ca anomaly in the topmost part of the core, which means this earthquake did not trigger any mass wasting. This example shows that earthquake-triggered subaqueous mass wasting events are unlikely in Ölüdeniz Lagoon. Besides, there were many earthquakes around Fethiye according to historical records, some of which are 1846 Hellenic arc, Mar 5 1851 Fethiye, Apr 3 1851 Fethiye, May 19 1852 Fethiye, Jul 18 1852 Fethiye, Feb 9 1855 Fethiye, Mar 2 1855 Fethiye and Feb 22 Fethiye (Ambraseys, 2009). On Mar 5 1851, there were many demolished buildings and losses of lives. On Apr 3 1851, the largest earthquake recorded in the region, caused the landslides and rockfalls to happen. The sea level rose and caused coastal flooding (Ambraseys, 2009). According to Antonopoulos, this earthquake created tsunami waves in 1.8 m height, flooded over the land. On Jul 18, 1852, earthquake caused deformation and liquefaction on the ground. Despite being such destructive earthquakes, none of these are seen in the cores. Thus, considering those historically and instrumentally recorded earthquakes, it can be understood that Ölüdeniz lagoon do not record any earthquake around the region, i.e., there is no soft-sediment deformation or mass-wasting. Probably only tsunamis are recorded, which were capable of carrying the sediments from sand spit/near shore to the middle of the lagoon.

Another mechanism that could create Ti/Ca anomalies would be flooding or heavy rain events. During floods, significant amounts of terrigenous clastics could well be transported in the lagoon, and suddenly deposited, and result in Ti/Ca anomalies. However, the catchment of Ölüdeniz Lagoon (Figure 1.8b) is quite small to create severe flooding that could result in basinwide intercalations showing Ti/Ca anomalies. In addition, the recurrence interval of Ti/Ca anomalies in Ölüdeniz sequence seems to be around 250-300 years. Heavy rain events causing flooding should be much more frequent than 250-300 years. Thus, flooding or heavy rain events are probably recorded as much smaller anomalies that could be barely distinguished from the background sediments.

Extreme Wave Events (EWE), i.e. storms, can also overwash the sand spit of the lagoon and create Ti/Ca anomalies as well. It is hard to differentiate storm deposits from tsunamigenic ones. However, still some clues have been used in evaluation whether it is storm or tsunami. For example, tsunamigenic deposits have bimodal deposition, fining-upward sequence and relatively thinner deposit layer than storm deposits, but storm deposits have poorly sorted relatively thicker deposits. However, since we do not see such clues in our study, we cannot evaluate in terms of those clues. In the cores, there is no lamination and almost all grains are in equal size. When we consider EWE condition in the eastern Mediterranean, Vött et al. (2018) state that tsunamis comprised 73–98% of all EWEs in the Mediterranean Sea for the period 1902–2017. These statistics suggest that the possibility that storm surges in the Mediterranean produce geological traces similar to those caused by tsunamis can be assumed to be insignificant (Avşar, 2019a). And hence, storms can be ruled out as well.

Due to the explanations above, and also given the fact that Ti/Ca anomalies temporally correlates with well-known historical tsunamis, one can say that the reason of sedimentary events in Ölüdeniz Lagoon is more likely tsunamis rather than other mechanisms such as storms, floods or earthquake-triggered mass wasting. Accordingly, sedimentary events are assumed to be of tsunami origin. Ti/Ca profiles along the Ölüdeniz cores are plotted with respect to time, and events are compared with historical and geological tsunami records in the region in Figure 4.9b. Accordingly, among the tsunamis triggered by the Hellenic Arc and Pliny-Strabo trenches, the ones in 1609 CE (I=8, Rhodes), 1303 CE (I=10, Heraklion), 365 CE (I=10, Alexandria) and 148 CE (I=7, Rhodes) were clearly recorded in Ölüdeniz Lagoon. On the other hand, there are no traces of the tsunamis in 1948 CE (I=7, Karpathos), 1741 CE (I=8, Rhodes), and 1481 CE (I=7, Rhodes). It looks like intensities around 8-9 is the threshold for Ölüdeniz Lagoon to record a tsunami clearly.

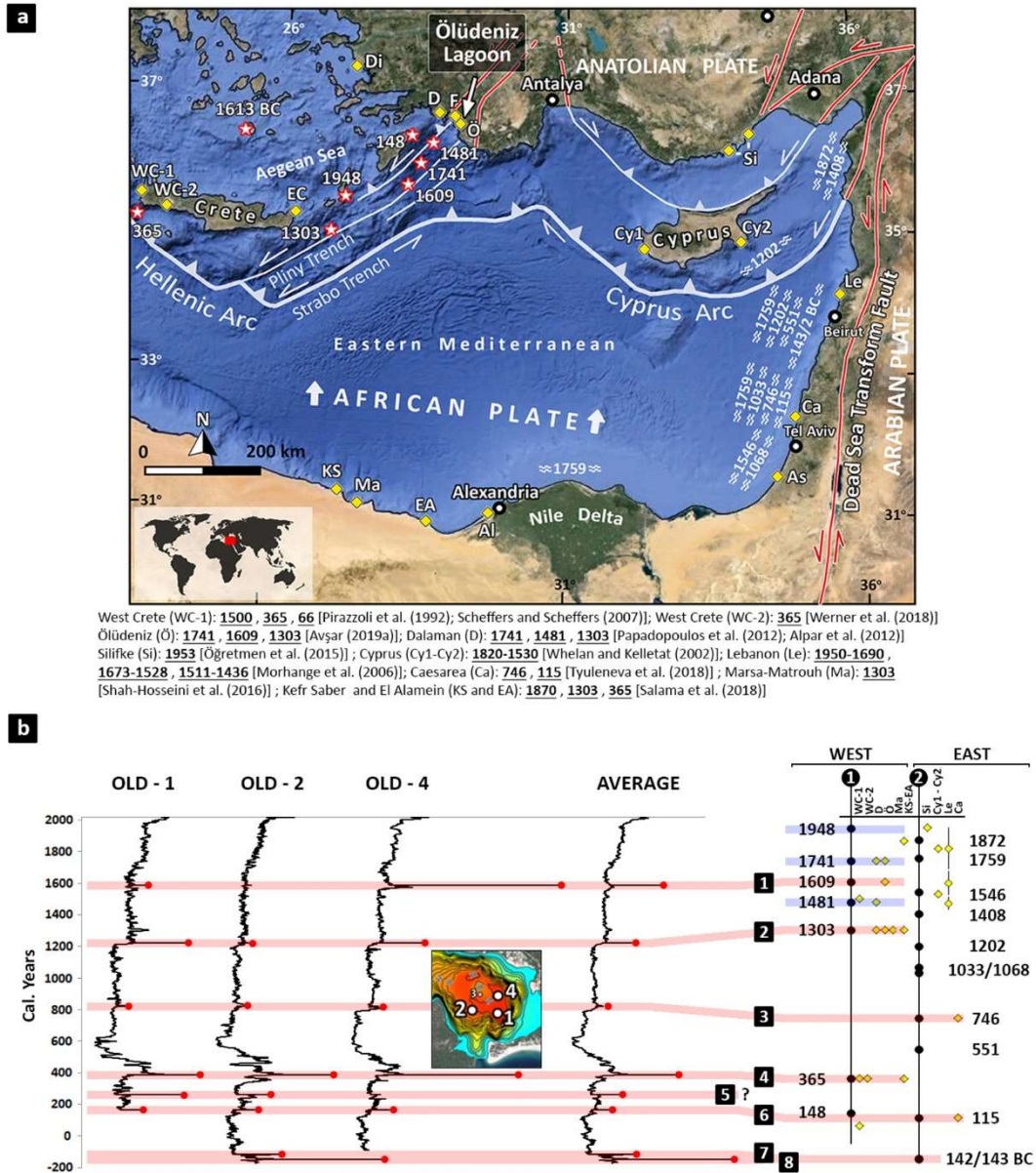


Figure 4.5. a) Historical tsunamis in the eastern Mediterranean and geological paleotsunami records (Yellow diamonds) (See Figure 2.1 for the legend) b) Comparison of sedimentary events (Ti/Ca anomalies) with historical tsunamis and paleotsunami records.

Event 5 was not recorded in OLD-4, while Event 1 was not recorded in OLD-2. Except these two events, all of the other events were recorded in all three cores. Thus, since they are not basin-wide, it can be said that Event 1 (i.e. 1609 CE tsunami) and Event 5 had less intensity than the other events in the Ölüdeniz

sedimentary record. Although, 148 CE tsunami (Event 6) had intensity of 7 at Rhodes (Table 2.1), which is lower than the intensity of 1609 CE tsunami (8 at Rhodes), it was recorded in all of the cores. 1741 CE and 1481 CE tsunamis have intensities at Rhodes as 8 and 7, respectively, (i.e., equal or higher than the intensity of 148 CE tsunami), but these tsunamis were not recorded in Ölüdeniz. This observation implies that 148 CE tsunami was stronger than thought.

Event 3 is recorded in all of the cores and approximately corresponds to 746 CE tsunami historically recorded along Israel coasts. Although it looks like a strong tsunami since it is seen in all cores, its intensity is just 7 along Levantine coasts (Table 2.1). It is highly unlikely that a tsunami of intensity 7 along Levantine coasts would travel all through the Mediterranean and recorded in Ölüdeniz. Whether its intensity was underestimated or this event was because of a tsunami closer to Ölüdeniz, but not recorded in history.

At the bottom of OLD-2, there are two events very closely spaced, i.e. events 7 and 8. According to the age-depth curve, these events temporally correspond to closely spaced tsunamis in 142 and 143 BCE along the coasts of Lebanon. These events also support the success of the age-depth model. Event 6 may also be correlated with the CE 115 tsunami in Israel, but CE 148 tsunami, which is much closer to Ölüdeniz, is more susceptible. Event 5, seen in OLD-1 and OLD-2, does not correspond any historically recorded tsunamis. It could have been sourced by an unwritten local tsunamigenic earthquake. Similarity of this event is also seen on Apr 3 1851 earthquake. This earthquake must have been local because it is not felt any other region out of Fethiye. Thus, tsunamigenic event clues remained weak for that event. In addition, none of the cores did record this event, although, historical records tell about 1.8 m tsunami wave and coastal flooding. Due to being local event, Event 5 may not also have been noticed or there was no inhabitant in the Fethiye region at those years.

Another important observation about the tsunami deposits in Ölüdeniz is that the event deposits do not contain distinctly coarser grains or macro-mollusk shell

remains that could be transported from the sand spit. Even in OLD-1, which is just 400 m from the sand spit, there is no significant change in grain-size. This means that tsunamis were not strong enough to transport mollusk shells for even 400 m. This implies that tsunamis in the eastern Mediterranean may not be as catastrophic as the ones in the Pacific and Indian oceans.

CHAPTER 5

CONCLUSION

The following conclusions can be drawn from this study:

- Collecting cores at multiple locations increases the chance of finding terrigenous organic material for radiocarbon dating. In addition, it strengthens interpretations through stratigraphical correlation of sediments at different locations,
- Since Ölüdeniz sediments do not contain laminations, u-channel radiography could not give any information about sedimentary structures. They are used to assess sediment densities and core correlation.
- The tsunami deposits in Ölüdeniz sedimentary sequence tend to be more reddish-brown compared to the yellowish-grey background sediments.
- The tsunami deposits are enriched in terrigenous elements like Ti, K, Fe, and Zn with respect to Ca, and are expressed as significant peaks along (Ti, K, Fe, Zn) / (Ca) profiles.
- Tsunami-related peaks along (Ti, K, Fe, Zn) / (Ca) profiles are explained as follows: During sudden deposition of clastics, which are overwashed from the sand spit, in the lagoon, there is not enough time for bio/chemical carbonate precipitation from the water column. This results in Ca-depleted intercalations within the background sediments.
- According to radiocarbon-based chronology, Ölüdeniz Lagoon recorded tsunamis related to 1609, 1303, 746, 365, 148 CE and 142&143 BCE events.
- The tsunami deposits do not contain coarser grains (gravel or pebble) or mollusk shells even within the core closest to the sand spit (OLD-1, approximately 400

m from the spit). This implies that the tsunamis were not strong enough to transport mollusk shells or gravel even for 400 m. Based on this observation, it can be concluded that tsunamis in the eastern Mediterranean are not as catastrophic as the ones in the Pacific and Indian oceans.

REFERENCES

- Akkar, S., & Çağnan, Z. (2010). A local ground-motion predictive model for Turkey, and its comparison with other regional and global ground-motion models. *Bulletin of the Seismological Society of America*, 100(6), 2978-2995.
- Allmann, A. (2012). Earthquake, tsunami, nuclear accident – The triple disaster of Tohoku. *Topics Geo 2012 Issue*, 7–11.
- Alpar, B., Ünlü, S., Altınok, Y., Özer, N., & Aksu, A. (2012). New approaches in assessment of tsunami deposits in Dalaman (SW Turkey). *Natural hazards*, 63(1), 181-195.
- Ambraseys, N. (2009). *Earthquakes in the Mediterranean and Middle East: A Multidisciplinary Study of Seismicity up to 1900*. Cambridge University Press, 968 pp.
- Avşar, U. (2013). *Lacustrine paleoseismic records from the North Anatolian Fault, Turkey* (Doctoral dissertation, Ghent University).
- Avşar, U., Jónsson, S., Geirsdóttir, Á., & Miller, G.H. (2013). Seeking information on pre-historic earthquakes near Húsavík in Lake Sediment Cores from Botnsvatn and Hoskuldsvatn. In: Johannesdóttir, G.B., R. Stefánsson, P. Einarsson, S. Jónsson (Eds.), *Proceedings of International Workshop on Earthquakes in North Iceland, 6-8 June 2013, Húsavík, Iceland*, 39-41.
- Avşar, U., Hubert-Ferrari, A., De Batist, M., Schmidt, S., & Fagel, N. (2015). Sedimentary records of past earthquakes in Boraboy Lake during the last ca 600 years (North Anatolian Fault, Turkey). *Palaeogeography Palaeoclimatology Palaeoecology* 433, 1-9.

- Avşar, U., Jonsson, S., Avşar, Ö., & Schmidt, S. (2016). Earthquake-induced soft-sediment deformations and seismically amplified erosion rates recorded in varved sediments of Köyceğiz Lake (SW Turkey). *Journal of Geophysical Research – Solid Earth* 121, 4767–4779.
- Avşar, U. (2019a). Sedimentary geochemical evidence of historical tsunamis in the Eastern Mediterranean from Ölüdeniz Lagoon, SW Turkey. *Journal of Paleolimnology* 61(3), 373-385.
- Avşar, U. (2019b). Sedimentary Traces of Tsunamis in the Aegean Sea during the Last 1500 Years, (Karine Lagoon, W Turkey). *Geological Bulletin of Turkey* 62(3), 199-220.
- Baba, M. (2013). Fukushima accident: What happened? *Radiation Measurements*, 55, 17–21.
- Bahlburg, H., & Spiske, M. (2012). Sedimentology of tsunami inflow and backflow deposits: key differences revealed in a modern example. *Sedimentology*, 59(3), 1063-1086.
- Barka, A., & Reilinger, R. (1997). Active tectonics of the Eastern Mediterranean region: deduced from GPS, neotectonic and seismicity data. *Ann Geophys Italy* 40, 587-610.
- Bertrand, S., Doner, L., Akçer Ön, S., Sancar, U., Schudack, U., Mischke, S., Çağatay, M.N., & Leroy, S.A.G. (2011). Sedimentary record of coseismic subsidence in Hersek coastal lagoon (Izmit Bay, Turkey) and the late Holocene activity of the North Anatolian Fault. *Geochem Geophys Geosy* 12, 1–17.
- Björck, S., & Wohlfarth, B. (2002). ^{14}C chronostratigraphic techniques in paleolimnology. In *Tracking environmental change using lake sediments* (pp. 205-245). Springer, Dordrecht.

- Borrero, J. C., Synolakis, C. E., & Fritz, H. (2006). Northern Sumatra Field Survey after the December 2004 Great Sumatra Earthquake and Indian Ocean Tsunami. *Earthquake Spectra*, 22(S3), 93– 104. doi:10.1193/1.2206793
- Bronk Ramsey, C. (2017). Oxcal Program V. 4.3.2". University of Oxford, Radiocarbon Accelerator Unit.
- Bruins, H.J., MacGillivray, J.A., Synolakis, C.E., Benjamini, C., Keller, J., Kisch, H.J., Klügel, A., & van der Plicht, J. (2008). Geoarchaeological tsunami deposits at Palaikastro (Crete) and the Late Minoan IA eruption of Santorini. *Journal of Archaeological Science* 35, 191–212.
- Bryant, E.A. (2008). *Tsunami: The underrated hazard*. 2nd edn. Berlin: Springer. doi:10.1007/s00024-009-0545-7.
- Clarke, F.W., & Washington, H.S. (1924). *The Composition of the Earth's Crust* (Vol. 127). US Government Printing Office.
- Chagué-Goff, C., Niedzielski, P., Wong, H.K.Y., Szczuciński, D., Sugawara, D., & Goff, J. (2012). Environmental impact assessment of the 2011 Tohoku-oki tsunami on the Sendai Plain. *Sedimentary Geology* 282, 175-187.
- Colombo, J. C., Silverberg, N., & Gearing, J. N. (1997). Lipid biogeochemistry in the Laurentian trough—II. Changes in composition of fatty acids, sterols and aliphatic hydrocarbons during early diagenesis. *Organic Geochemistry*, 26(3-4), 257-274.
- Croudace, I. W., Rindby, A., & Rothwell, R. G. (2006). ITRAX: description and evaluation of a new multi-function X-ray core scanner. *Geological Society, London, Special Publications*, 267(1), 51-63.
- Daniell, J., & Vervaeck, A. (2012). Damaging earthquakes 1568 database 2011—The year in review. http://www.cedim.de/download/1569_CATDATDamagingEarthquakesDatabase2011AnnualReview.pdf. 2015-10-15.

- Darling, D. (2007). Elements, Terrestrial Abundance. Retrieved From <https://Web.Archive.Org/Web/20070410165310/Http://Daviddarling.Info/Encyclopedia/E/Elterr.Html>
- Dawson, A.G., & Stewart, I. (2007). Tsunami deposits in the geological record. *Sedimentary Geology* 200(3-4), 166-183.
- Dezileau, L., Sabatier, P., Blanchemanche, P., Joly, B., Swingedouw, D., Cassou, C., ... & Von Grafenstein, U. (2011). Intense storm activity during the Little Ice Age on the French Mediterranean coast. *Palaeogeography, Palaeoclimatology, Palaeoecology*, 299(1-2), 289-297.
- Dezileau, L., & Castaings, J. (2014). Extreme storms during the last 500 years from lagoonal sedimentary archives in Languedoc (SE France). *Méditerranée. Revue géographique des pays méditerranéens/Journal of Mediterranean geography*, (122), 131-137.
- Dewey, J. F., & ŞENGÖR, A. C. (1979). Aegean and surrounding regions: complex multiplate and continuum tectonics in a convergent zone. *Geological Society of America Bulletin*, 90(1), 84-92.
- Dominey-Howes, D.T.M., Humphreys, G.S., & Hesse, P.P., (2006), Tsunami and palaeotsunami depositional signatures and their potential value in understanding the late-Holocene tsunami record: *The Holocene*, v. 16, p. 1095, doi: 10.1177/0959683606069400.
- Donato, S.V., Reinhardt, E.G., Boyce, J.I., Rothaus, R., & Vosmer, T., (2008), Identifying tsunami deposits using bivalve shell taphonomy: *Geology*, v. 36, p. 199–202, doi: 10.1130/G24554A.1.
- Dura, T., Cisternas, M., Horton, B. P., Ely, L. L., Nelson, A. R., Wesson, R. L., & Pilarczyk, J. E. (2015). Coastal evidence for Holocene subduction-zone earthquakes and tsunamis in central Chile. *Quaternary Science Reviews*, 113, 93-111.

- Eddy, C., & Sase, E. (2015). Implications of the Fukushima Nuclear Disaster: Man-Made Hazards, Vulnerability Factors, and Risk to Environmental Health. *Journal of Environmental Health* 78, 26-32.
- Emre, Ö., Doğan, A., & Özalp, S. (2011). 1:250.000 Ölçekli Türkiye Diri Fay Haritaları Serisi. Maden Tetkik ve Arama Genel Müdürlüğü, Ankara-Türkiye.
- Emery, G. R., & Broussard, D. E. F. (1954). A modified Kullenberg piston corer. *Journal of Sedimentary Research*, 24(3), 207-211.
- FAO, (2007). The State of World Fisheries and Aquaculture. Food and Agriculture Organization of the United Nations Publication. Rome, 222 pp.
- FAO, (2010). The State of World Fisheries and Aquaculture. Food and Agriculture Organization of the United Nations Publication. Rome, 197pp.
- FAO, (2014). The State of World Fisheries and Aquaculture. Food and Agriculture Organization of the United Nations Publication. Rome, 223 pp.
- FAO, (2018). The State of World Fisheries and Aquaculture. Food and Agriculture Organization of the United Nations Publication. Rome, 210 pp.
- Fischer, P., Finkler, C., Röbbke, B.R., Baika, K., Hadler, H., Willershauser, T., Rigakou, D., Metallinou, G., & Vött, A. (2016). Impact of Holocene tsunamis detected in lagoonal environments on Corfu (Ionian Islands, Greece) - geomorphological, sedimentary and microfaunal evidence. *Quaternary International* 401, 4–16.
- Fritz, H.M., Mohammed, F., & Yoo, J. (2009). Lituya Bay landslide impact generated mega-tsunami 50th Anniversary. In *Tsunami Science Four Years after the 2004 Indian Ocean Tsunami* (pp. 153-175). Birkhäuser Basel.

- Goff, J., Lamarche, G., Pelletier, B., Chague-Goff, C., & Strotz, L. (2011). Predecessors to the 2009 South Pacific tsunami in the Wallis and Futuna archipelago. *Earth Science Reviews* 107, 91-106.
- Goodman-Tchernov, B. N., Dey, H. W., Reinhardt, E. G., McCoy, F., & Mart, Y. (2009). Tsunami waves generated by the Santorini eruption reached Eastern Mediterranean shores. *Geology*, 37(10), 943-946.
- Govers, R., & Wortel, M.J.R. (2005). Lithosphere tearing at STEP faults: Response to edges of subduction zones. *Earth and Planetary Letters*, 236, 505-523.
- Graehl, N.A., Kelsey, H.M., Witter, R.C., Hemphill-Haley, E., & Engelhart, S.E., (2015). Stratigraphic and microfossil evidence for a 4500-year history of Cascadia subduction zone earthquakes and tsunamis at Yaquina River estuary, Oregon, USA. *Geol Soc Am Bull* 127, 211–226.
- Gusiakov, V.K. (2009). Tsunami history: recorded. *The Sea* 15, 23-53.
- Hadler, H., Willershauser, T., Ntageretzi, K., Henning, P., & Vött, A. (2012). Catalogue entries and non-entries of earthquake and tsunami events in the Ionian Sea and the Gulf of Corinth (eastern Mediterranean, Greece) and their interpretation with regard to palaeotsunami research. In: Vött, A and Venzke, J.F. (eds) *Jahrestagung des Arbeitskreises "Geographie der Meere und Küsten"*, vol 44. Bremer Beiträge zur Geographie und Raumplanung, Bremen, pp 1–15.
- Hall, J., Aksu, A. E., Elitez, I., Yaltrak, C., & Çifçi, G. (2014). The Fethiye–Burdur Fault Zone: a component of upper plate extension of the subduction transform edge propagator fault linking Hellenic and Cyprus Arcs, Eastern Mediterranean. *Tectonophysics*, 635, 80-99.
- Helene, O., & Yamashita, M. T. (2006). Understanding the tsunami with a simple model. *European Journal of Physics*, 27(4), 855–863. doi:10.1088/0143-0807/27/4/016

- Hoffmann, N., Master, D., & Goodman-Tchernov, B. (2018). Possible tsunami inundation identified amongst 4–5th century BCE archaeological deposits at Tel Ashkelon, Israel. *Marine Geology* 396, 150-159.
- Hughes, J. F., Mathewes, R. W., & Clague, J. J. (2002). Use of pollen and vascular plants to estimate coseismic subsidence at a tidal marsh near Tofino, British Columbia. *Palaeogeography, Palaeoclimatology, Palaeoecology*, 185(1-2), 145-161.
- Imamura, A. (1937), *Theoretical and Applied Seismology*. Maruzen, Tokyo.
- Iskander, M.M. (2013). Wave climate and coastal structures in the Nile delta coast of Egypt. *Emir J Eng Res* 18(1), 43–57.
- Kaymakçı, N., Langereis, C., Özkaptan, M., Özacar, A. A., Gülyüz, E., Uzel, B., & Sözbilir, H. (2018). Paleomagnetic evidence for upper plate response to a STEP fault, SW Anatolia. *Earth and Planetary Science Letters*, 498, 101-115.
- Kelsey, H. M., Nelson, A. R., Hemphill-Haley, E., & Witter, R. C. (2005). Tsunami history of an Oregon coastal lake reveals a 4600 yr record of great earthquakes on the Cascadia subduction zone. *Geological Society of America Bulletin*, 117(7-8), 1009-1032.
- Kempf, P., Moernaut, J., Van Daele, M., Vandoorne, W., Pino, M., Urrutia, R., & De Batist, M. (2017). Coastal lake sediments reveal 5500 years of tsunami history in south central Chile. *Quaternary Science Reviews*, 161, 99-116.
- Le Pichon, X., & Kreemer, C. (2010). The Miocene-to-present kinematic evolution of the Eastern Mediterranean and Middle East and its implications for dynamics. *Annual Review of Earth and Planetary Sciences*, 38, 323-351.
- Mamo, B., Strotz, L., & Dominey-Howes, D. (2009). Tsunami sediments and their foraminiferal assemblages. *Earth-Science Reviews*, 96(4), 263-278.

- Marriner, N., Kaniewski, D., Morhange, C., Flaux, C., Giaime, M., Vacchi, M., & Goff, J. (2017). Tsunamis in the geological record: Making waves with a cautionary tale from the Mediterranean. *Science advances*, 3(10), e1700485.
- Mathes-Schmidt, M., Schwarzbauer, J., Papanikolaou, I., Syberberg, F., Thiele, A., Wittkopp, F., & Reicherter, K. (2013). Geochemical and micropaleontological investigations of tsunamigenic layers along the Thracian Coast (Northern Aegean Sea, Greece). *Zeitschrift für Geomorphologie, Supplementary Issues*, 57(4), 5-27.
- McCoy, F. W., & Heiken, G. (2000). Tsunami generated by the Late Bronze age eruption of Thera (Santorini), Greece. *Pure and Applied Geophysics*, 157(6-8), 1227-1256.
- McCoy, F., Synolakis, C.E., & Papadopoulos, G.A. (2000), Tsunami generated during the LBA eruption of Thera—Evidence from modelling and sedimentary deposits: *Eos (Transactions, American Geophysical Union)*, v. 81, abs. T21E-13.
- McCurry, J. (2013). Fukushima residents still struggling 2 years after disaster. *The Lancet*, 381(9869), 791–792.
- McKenzie, D. (1972). Plate tectonics in the Mediterranean region. *Nature*, 226, 239-243.
- McLeod, M.K., Slavich, P.G., Irhas, Y., Moore, N., Rachman, A., Ali, N., Iskandar, T., Hunt, C. & Caniango, C. (2010). Soil salinity in Aceh after the December 2004 Indian Ocean tsunami. *Agricultural Water Management* 97(5), 605-613.
- Migeon, S., Weber, O., Faugeres, J. & Saint-Paul, J. (1999). SCOPIX: a new X-ray imaging system for core analysis. *Geo-Marine Letters* 18, 251–255.
- Minoura, K., Imamura, F., Kuran, U., Nakamura, T., Papadopoulos, G.A., Takahashi, T. & Yalciner, A.C. (2000). Discovery of Minoan tsunami deposits. *Geology* 28(1), 59-62.

- Mischke, S., Schudack, U., Bertrand, S., & Leroy, S.A.G. (2012). Ostracods from a Marmara Sea lagoon (Turkey) as tsunami indicators. *Quaternary International* 261, 156–161.
- Mook, W.G. (1986). Recommendations/Resolutions Adopted by the 12th International Radiocarbon Conference. *Radiocarbon* 28, 799.
- Morhange, C., Marriner, N. & Pirazzoli, P.A. (2006). Evidence of Late-Holocene tsunami events in Lebanon. *Zeitschrift für Geomorphologie NF* 146, 81-95.
- Morton, R.A., Gelfenbaum, G., & Jaffe, B.E. (2007). Physical criteria for distinguishing sandy tsunami and storm deposits using modern examples. *Sedimentary Geology* 200, 184-207.
- Mori, N., Takahashi, T., Yasuda, T., & Yanagisawa, H. (2011). Survey of 2011 Tohoku earthquake tsunami inundation and run-up. *Geophysical Research Letters* 38(7), L00G14 1-6.
- National Geophysical Data Center / World Data Service (NGDC/WDS), (2019). Global Historical Tsunami Database. National Geophysical Data Center, NOAA.
- Nanayama, F., Furukawa, R., Kiyoyuki, S., Makino, A., Soeda, Y., & Igarashi, Y. (2007). Nine unusually large tsunami deposits from the past 4000 years at Kiritappu marsh along the southern Kuril Trench. *Sedimentary Geology* 200, 275–294.
- Olsson, I. (1991). Accuracy and Precision in Sediment Chronology. *Hydrobiologia* 214, 25-34.
- Ocakoglu, N. (2012). Investigation of Fethiye-Marmaris Bay (SW Anatolia): seismic and morphologic evidences from the missing link between the Pliny Trench and the Fethiye-Burdur Fault Zone. *Geo-Marine Letters* 32, 17-28.

- Oskin, B. (2017). Japan Earthquake & Tsunami of 2011: Facts and Information. Retrieved October 25, 2019, from <https://www.livescience.com/39110-japan-2011-earthquake-tsunami-facts.html>.
- Öğretmen, N., Cosentino, D., Gliozzi, E., Cipollari, P., Iadanza, A. & Yildirim, C. (2015). Tsunami hazard in the Eastern Mediterranean: geological evidence from the Anatolian coastal area (Silifke, southern Turkey). *Natural Hazards* 79(3), 1569-1589.
- Özbakır, A.D., Şengör, A.M.C., Wortel, M.J.R., & Govers, R. (2013). The Pliny-Strabo trench region: a large shear zone resulting from slab tearing. *Earth and Planetary Science Letters* 375, 188-195.
- Papadopoulos, G.A., & Imamura, F. (2001). A proposal for a new tsunami intensity scale. *Proceedings of ITS-2001* 5, 569-577.
- Papadopoulos, G., Minoura, K., Imamura, F., Kuran, U., Yalçiner, A., Fokaefs, A., & Takahashi, T. (2012). Geological evidence of tsunamis and earthquake at the Eastern Hellenic Arc: correlation with historical seismicity in the eastern Mediterranean Sea. *Research in Geophysics* 2(2), e12-e12.
- Papadopoulos, G.A., Gràcia, E., Urgeles, R., Sallares, V., De Martini, P.M., Pantosti, D., González, M., Yalçiner, A.C., Mascle, J., Sakellariou, D., Salamon, A., Tinti, S., Karastathis, V., Fokaefs, A., Camerlenghi, A., Novikova, T., & Papageorgiou, A. (2014). Historical and pre-historical tsunamis in the Mediterranean and its connected seas: Geological signatures, generation mechanisms and coastal impacts. *Marine Geology* 354, 81-109.
- Papadopoulos, G. (2016). Tsunamis in the Global Ocean. In: Papadopoulos, G. (ed), *Tsunamis in the European-Mediterranean Region*, Elsevier, 2016, Pages 1-37.

- Parrish, C.C., Abrajano, T.A., Budge, S.M., Helleur, R.J., Hudson, E.D., Pulchan, K., & Ramos, C. (2000). Lipid and phenolic biomarkers in marine ecosystem: analysis and applications. In: PJ Wangersky (ed) *Marine chemistry. The handbook of environmental chemistry*, vol 5D. Springer, Berlin, pp 193–223.
- Pilarczyk, J.E., & Reinhardt, E.G. (2012). Testing foraminiferal taphonomy as a tsunami indicator in a shallow arid system lagoon: Sur, Sultanate of Oman. *Marine Geology* 295–298, 128–136.
- Pirazzoli, P.A., Ausseil-Badie, J., Giresse, P., Hadjidaki, E., & Arnold, M. (1992). Historical environmental changes at Phalasarna harbor, West Crete. *Geoarchaeology* 7(4), 371-392.
- Pirazzoli, P.A. (2005). A review of possible eustatic, isostatic and tectonic contributions in eight late-Holocene relative sea-level histories from the Mediterranean area. *Quaternary Science Reviews* 24(18-19), 1989-2001.
- Razjigaeva, N. G., Ganzey, L. A., Grebennikova, T. A., Ivanova, E. D., Kharlamov, A. A., Kaistrenko, V. M., ... & Chernov, S. B. (2014). The Tohoku Tsunami of 11 March 2011: The key event to understanding tsunami sedimentation on the coasts of closed bays of the Lesser Kuril Islands. *Pure and Applied Geophysics*, 171(12), 3307-3328.
- Reimer, P.J. (2013). Intcal13 and Marine13 Radiocarbon Age Calibration Curves, 0-50,000 Years Cal BP. *Radiocarbon* 55 (4), 1869-1887.
- Reinhardt, E. G., Goodman, B. N., Boyce, J. I., Lopez, G., van Hengstum, P., Rink, W. J., ... & Raban, A. (2006). The tsunami of 13 December AD 115 and the destruction of Herod the Great's harbor at Caesarea Maritima, Israel. *Geology*, 34(12), 1061-1064.
- Röbke, B. R., & Vött, A. (2017). The tsunami phenomenon. *Progress in Oceanography*, 159, 296-322.

- Ruiz, F., Abad, M., Cáceres, L. M., Vidal, J. R., Carretero, M. I., Pozo, M., & González-Regalado, M. L. (2010). Ostracods as tsunami tracers in Holocene sequences. *Quaternary Research*, 73(1), 130-135.
- Sabatier, P., Dezileau, L., Colin, C., Briquieu, L., Bouchette, F., Martinez, P., ... & Von Grafenstein, U. (2012). 7000 years of paleostorm activity in the NW Mediterranean Sea in response to Holocene climate events. *Quaternary Research*, 77(1), 1-11.
- Salama, A., Meghraoui, M., Gabry, M. E., Maouche, S., Hussein, M. H., & Korrat, I. (2018). Paleotsunami deposits along the coast of Egypt correlate with historical earthquake records of eastern Mediterranean. *Natural Hazards and Earth System Sciences*, 18(8), 2203-2219.
- Salamon, A., Rockwell, T., Ward, S. N., Guidoboni, E., & Comastri, A. (2007). Tsunami hazard evaluation of the eastern Mediterranean: historical analysis and selected modeling. *Bulletin of the Seismological Society of America*, 97(3), 705-724.
- Scheffers, A., & Kelletat, D. (2004). Bimodal tsunami deposits—a neglected feature in paleo-tsunami research. *Coastline Reports*, 1, 67-75.
- Scheffers, A., & Scheffers, S. (2007). Tsunami deposits on the coastline of west Crete (Greece). *Earth and Planetary Science Letters* 259(3-4), 613-624.
- Shah-Hosseini, M., Saleem, A., Mahmoud, A. M. A., & Morhange, C. (2016). Coastal boulder deposits attesting to large wave impacts on the Mediterranean coast of Egypt. *Natural Hazards*, 83(2), 849-865.
- Shotton, F.W. (1972). An Example of Hard-Water Error in Radiocarbon Dating of Vegetable Matter. *Nature* 240(5382), 460-461.
- Smedile, A., De Martini, P. M., Pantosti, D., Bellucci, L., Del Carlo, P., Gasperini, L., ... & Boschi, E. (2011). Possible tsunami signatures from an integrated study in the Augusta Bay offshore (Eastern Sicily—Italy). *Marine Geology*, 281(1-4), 1-13.

- Stanley, J. D., & Pia Bernasconi, M. (2006). Holocene depositional patterns and evolution in Alexandria's Eastern Harbor, Egypt. *Journal of Coastal Research*, 283-297.
- Stefens, J. L., dos Santos, J. H. Z., Mendonça Filho, J. G., da Silva, C. G. A., & Ruaro Peralba, M. D. C. (2007). Lipid biomarkers profile—presence of coprostanol: recent sediments from Rodrigo de Freitas Lagoon—Rio de Janeiro, Brazil. *Journal of Environmental Science and Health, Part A*, 42(11), 1553-1560.
- Stuiver, M., & Polach, H. A. (1977). Discussion reporting of ^{14}C data. *Radiocarbon*, 19(3), 355-363.
- Sugawara, D., Minoura, K., & Imamura, F. (2008). Tsunamis and tsunami sedimentology. In *Tsunamiites* (pp. 9-49). Elsevier.
- Şenel, M. (1997). Geological Map Series of Turkey 1:100 000 scale. No. 2, Geologic Map of Fethiye L8 Quadrangle. General Directorate of Mineral Research and Exploration, Geological Research Department, Ankara (in Turkish).
- Türk – Endonezya İş Konseyi Endonezya Ülke Bülteni Ağustos (2014). Ankara, Dış Ekonomik İlişkiler Kurulu (DEİK). 19 pp. (in Turkish)
- Tosun, L. (2018). Active Tectonics and Kinematics of Fethiye-Göcek Bay, SW Turkey (Doctoral Dissertation, Middle East Technical University).
- Tsuji, Y., Okamura, M., Matsuoka, H., Goto, T., & Hang, S. (2002). Traces of historical and prehistorical tsunamis in the lake-bottom sedimentary sequences at Oh-Ike (Owase City) and Suwa-Ike (Kii-Nagashima Town), Mie Prefecture. *Chikyū Monthly* 280, 743–747. (In Japanese)
- Villholth, K. G., & Neupane, B. (2011). Tsunamis as long-term hazards to coastal groundwater resources and associated water supplies. In *Tsunami-A growing disaster*. IntechOpen.

- Vött, A., Brückner, H., May, S. M., Sakellariou, D., Nelle, O., Lang, F., ... & Fountoulis, I. (2009). The Lake Voulkaria (Akarnania, NW Greece) palaeoenvironmental archive—a sediment trap for multiple tsunami impact since the mid-Holocene. *Zeitschrift für Geomorphologie, Supplementary Issues*, 53(1), 1-37.
- Vött, A., Lang, F., Brückner, H., Gaki-Papanastassiou, K., Maroukian, H., Papanastassiou, D., ... & Willershäuser, T. (2011). Sedimentological and geoarchaeological evidence of multiple tsunamigenic imprint on the Bay of Palairos-Pogonia (Akarnania, NW Greece). *Quaternary International*, 242(1), 213-239.
- Vött, A., Bruins, H. J., Gawehn, M., Goodman-Tchernov, B. N., De Martini, P., M., Kelletat, D., ... & Willershäuser, T. (2018). Publicity waves based on manipulated geoscientific data suggesting climatic trigger for majority of tsunami finding in the Mediterranean – Response to 'Tsunamis in the geological record: Making waves with a cautionary tale from the Mediterranean' by Marriner et al. (2017). *Zeitschrift für Geomorphologie, Supplementary Issues*, 62(2), 7-45.
- Werner, V., Baika, K., Fischer, P., Hadler, H., Obrocki, L., Willershäuser, T., & Emde, K., (2018). The sedimentary and geomorphological imprint of the AD 365 tsunami on the coasts of southwestern Crete (Greece)—Examples from Sougia and Palaiochora. *Quaternary International* 473, 66-90.
- Whelan, F., & Kelletat, D. (2002). Geomorphic evidence and relative and absolute dating results for tsunami events on Cyprus. *Science of Tsunami Hazards* 20(1), 3-16.
- Willershäuser, T., Vött, A., Hadler, H., Ntageretzis, N., Emde, K., & Brückner, H. (2015). Holocene palaeotsunami imprints in the stratigraphical record and the coastal geomorphology of the Gialova Lagoon near Pylos (southwestern Peloponnese, Greece). *Z Geomorphol (Supp Vol)* 59(4), 215–252.
- World Bank. (2005). World Bank response to the Tsunami disaster (English). Washington, DC: World Bank. <http://documents.worldbank.org/curated/en/194061468258308532/World-Bank-response-to-the-Tsunami-disaster>.

Yokoyama, I. (1978). The tsunami caused by the prehistoric eruption of Thera, in Doulas, C., eds., Thera and the Aegean World I: Second International Scientific Congress Papers: London, The Thera Foundation, p. 277–283.

Yolsal, S., Taymaz, T., & Yalçiner, A.C. (2007). Understanding tsunamis, potential source regions and tsunami-prone mechanisms in the Eastern Mediterranean. In Taymaz, T., et al. (eds) The Geodynamics of the Aegean and Anatolia. Geological Society, London, Special Publications 291, 201-230
man, Ö. And Chorowicz, J. 2002. Late Cenozoic tectonics and volcanics in the northwestern corner of the Arabian plate: a consequence of the strike-slip Dead Sea Fault Zone and lateral escape of Anatolia, Journal of Volcanology and Geothermal Research 117, 327-345.